UNIVERSIDADE FEDERAL DO PARANÁ

MARCOS VINICIUS LIMA DUNAJSKI

# IMPROVEMENT OF A LOW-COST TURBIDIMETER DESIGNED FOR ALGAE IDENTIFICATION

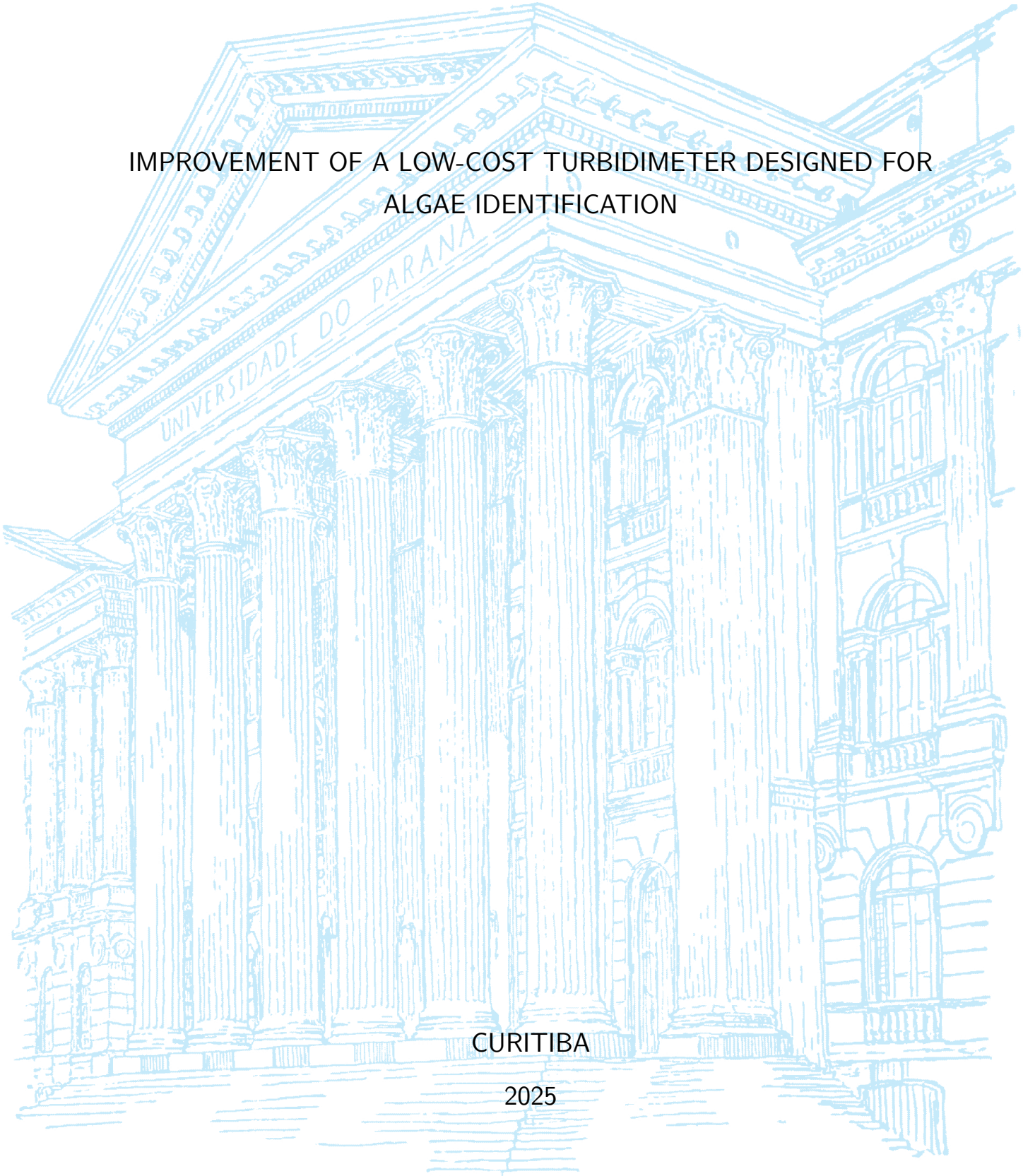


CURITIBA

2025

MARCOS VINICIUS LIMA DUNAJSKI

# IMPROVEMENT OF A LOW-COST TURBIDIMETER DESIGNED FOR ALGAE IDENTIFICATION

Trabalho de Conclusão de Curso de Graduação em Engenharia Ambiental, Setor de Tecnologia da Universidade Federal do Paraná, como requisito à obtenção do título de bacharel em Engenharia Ambiental.

Orientador:
Dr. Tobias Bleninger
Co-orientador:
Dr. Rafael de Carvalho Bueno

CURITIBA
2025

# RESUMO

Turbidez é um dos principais parâmetros adotados na avaliação da qualidade da água, por estar associada à presença de material orgânico e inorgânico em suspensão. A aderência de contaminantes a essas partículas pode prejudicar a desinfecção da água, reduzindo a eficácia na remoção de patógenos e representando riscos à saúde. Além disso, aumentos na turbidez de um corpo hídrico podem estar associados a processos como eutrofização, erosão e despejos pontuais. Avanços recentes na área de sensoriamento têm buscado ampliar o monitoramento desse parâmetro com o desenvolvimento de sensores de baixo custo. Tais sensores podem ser adotados não apenas para estimar a turbidez, mas também para identificar a origem do material particulado, permitindo distinguir a turbidez proveniente de algas e sedimentos e, assim, fornecer subsídios para a inferência do grau de eutrofização de corpos d'água. Este estudo tem como objetivo apresentar o desenvolvimento e avaliação de um protótipo óptico de baixo custo para a medição da turbidez em corpos d'água, com foco na detecção de algas. O protótipo opera no princípio nefelométrico, com um LED RGB programado para emitir três cores (verde, vermelho e branco) posicionado perpendicularmente a um sensor TCS230, capaz de captar a luz em diferentes faixas do espectro óptico e converter em um sinal de frequência. O sensor foi calibrado utilizando solução padrão de formazina, para dois intervalos distintos de turbidez, $0 - 80$ NTU e $80 - 200$ NTU, com o segundo apresentando um desempenho levemente superior, abrangendo curvas de calibração com coeficiente de determinação ($R^2$) médio de $0.990 \pm 0.003$, enquanto o intervalo inferior apresentou um $R^2$ médio de $0.985 \pm 0.005$. Considerando o intervalo análisado completo ($0 - 200$ NTU), para a validação, realizada com nova amostragem, foram obtidos valores médios de raiz do erro quadrático médio (RMSE), erro absoluto médio (MAE) e erro percentual absoluto médio (MAPE) de $7.4390 \pm 0.5253$ NTU, $4.4856 \pm 0.4089$ NTU e $8.8887 \pm 1.8514$ %, respectivamente, demonstrando desempenho comparável ao de outros turbidímetros de baixo custo. Para avaliar a eficácia do protótipo para a identificação de algas, uma série de testes foram realizados e revelaram respostas ópticas distintas em relação à formazina. A partir da adoção da razão entre as frequências obtidas para diferentes espectros ópticos, o sensor conseguiu distinguir entre diferentes fontes de turbidez e concentrações de clorofila para valores próximos ou acima de 5 NTU. Testes de monitoramento contínuo indicaram que a sonda consegue acompanhar tendências de variação de turbidez, embora apresente atraso de resposta para vazões mais acentuadas, especialente durante fases de diluição, com a redução gradual da turbidez. Embora durante estes testes, o modelo de estimativa de clorofila não tenha alcançado uma quantificação precisa em condições dinâmicas, a sonda detectou com sucesso aumentos significativos de clorofila associados à injeção de algas, demonstrando a viabilidade para identificação qualitativa de eventos semelhantes a florações de algas. De forma geral, os resultados mostram que a sonda óptica de baixo custo proposta pode distinguir diferentes fontes de turbidez sob condições controladas e detectar aumentos significativos de clorofila, mantendo precisão comparável à de outros protótipos de baixo custo.

**Palavras-chaves**: Turbidez; Sensoriamento remoto; Algas.

# ABSTRACT

Turbidity is one of the main parameters used in water-quality assessment, being associated with the presence of suspended organic and inorganic material. The adhesion of contaminants to these particles can impair water disinfection, reducing the effectiveness of pathogen removal and posing risks to human health. In addition, increases in the turbidity of a water body may be associated with processes such as eutrophication, erosion, and point-source discharges. Recent advances in sensing technologies have sought to expand the monitoring of this parameter through the development of low-cost sensors. Such sensors can be used not only to estimate turbidity but also to identify the origin of the particulate material, allowing the distinction between turbidity caused by algae and sediments and thereby supporting the inference of eutrophication levels in water bodies. This study aims to present the development and evaluation of a low-cost optical prototype for turbidity measurement in water bodies, with a focus on algae detection. The prototype operates on the nephelometric principle, with an RGB LED programmed to emit three colors (green, red, and white) positioned perpendicular to a TCS230 sensor, capable of capturing light in different regions of the optical spectrum and converting it into a frequency signal. The sensor was calibrated using a standard formazin solution for two distinct turbidity ranges, $0 - 80$ NTU and $80 - 200$ NTU, with the second range showing slightly superior performance, presenting calibration curves with an average coefficient of determination ($R^2$) of $0.990 \pm 0.003$, while the lower range presented an average $R^2$ of $0.985 \pm 0.005$. Considering the complete analyzed range ($0-200$ NTU), for the validation performed with a new sampling set, average values of root mean square error (RMSE), mean absolute error (MAE), and mean absolute percentage error (MAPE) of $7.4390 \pm 0.5253$ NTU, $4.4856 \pm 0.4089$ NTU and $8.8887 \pm 1.8514$ %, respectively, were obtained, demonstrating performance comparable to other low-cost turbidimeters. To evaluate the effectiveness of the prototype for algae identification, a series of tests were conducted and revealed optical responses distinct from those for formazin. By using the ratio between the frequencies obtained for different optical spectra, the sensor was able to distinguish between different turbidity sources and chlorophyll concentrations for values close to or above 5 NTU Continuous monitoring tests indicated that the probe can track turbidity-variation trends, although it presents response lag at higher flow rates, especially during dilution phases, when turbidity decreases gradually. Although in these tests the chlorophyll estimation model did not achieve precise quantification under dynamic conditions, the probe successfully detected significant increases in chlorophyll associated with algae injection, demonstrating feasibility for qualitative identification of bloom-like events. Overall, the results show that the proposed low-cost optical probe can distinguish between different turbidity sources under controlled conditions and detect significant increases in chlorophyll, while maintaining precision comparable to other low-cost prototypes.



**Key-words**: Turbidity; Remote sensing; Algae.

# List of Figures

# List of Tables

# Contents

# 1 Introduction

Water resources are vital for human life, with safe drinking water constituting an inalienable human right (United Nations, 1948). International efforts have been undertaken with a focus on universalizing access to this essential resource, regardless of geographical location or socioeconomic conditions (United Nations, 2015). In addition to ensuring access, it is essential to guarantee water quality and potability, which can be assessed using a wide range of physical, chemical and biological parameters, including, among others, pH, dissolved oxygen, electrical conductivity, temperature, turbidity, nutrient concentrations (e.g., total nitrogen and phosphorus), biochemical oxygen demand (BOD), and chlorophyll-a concentration.

While many of these parameters provide valuable insight into water quality, several require laboratory-based analytical methods, such as: nutrient quantification, microbiological analysis, or pigment extraction. These methods are often expensive, time-consuming, and incompatible with continuous, in situ monitoring, limiting the ability to promptly detect changes in water quality. In this context, turbidity stands out, as it can be easily monitored with sensors, providing relevant information about water quality, as it is associated with water cloudiness caused by suspended particles of either organic or inorganic origin.

Even inert particles, which would not normally pose a risk to potability, can adsorb contaminants and pathogens due to their large surface area (O'MELIA, 1980), thereby hindering water disinfection and reducing the efficiency of microorganism removal (CHRISTENSEN; LINDEN, 2003). Furthermore, turbidity can negatively impact domestic, industrial, and recreational uses of water resources (DROUJKO; MOLNAR, 2021; SANTOS, 2022). Thus, large amounts of suspended solids represent a potential source of water contamination and, consequently, a concern for water quality, with recent studies indicating a growing risk of gastrointestinal infections associated with high turbidity events (World Health Organization, 2017b).

In recent years, several studies have proposed low-cost turbidity sensors as a viable alternative for expanding monitoring networks. Works by Kelley et al. (2014), Gillett and Marchiori (2019), Rocher et al. (2021) and Droujko and Molnar (2021) demonstrated the technical feasibility of prototypes based on optical principles, using LED light sources and optical detectors to measure light scattering or absorption by suspended particles. However, most of these studies focus solely on the quantification of turbidity (in $NTU$) or solids concentration, without exploring the potential to identify the source of the particulate matter.

One notable exception is the study by Parra et al. (2018), who developed an optical sensor based on the Beer-Lambert law using multiple LEDs (red, green, yellow, and infrared) and dual detectors (LDR and photodiode). Their system was tested with river sediments and two microalgae species (Isochrysis galbana and Tetraselmis chui), and results showed that for turbidity levels above 12 NTU, it was possible to differentiate between turbidity sources based on the emitted wavelength. Nonetheless, this approach has limitations, including its narrow scope (focused on aquaculture), the need for specific calibration curves for each particle type, and the absence of continuous or field testing. Therefore, while preliminary efforts exist to assess the origin of turbidity, there remains a significant gap in the development of low-cost sensors that combine continuous measurement capability with source discrimination.

Given the importance of turbidity as a highly useful indicator, capable of providing valuable information about water quality quickly and continuously through the detection of suspended solids, which may be associated with watershed erosion, point source pollution, eutrophication, among other

factors, and considering the scarcity of affordable turbidimeter models available on the market, this study proposes the calibration and enhancement of an existing optical prototype (BUENO et al., 2023; DUNAJSKI et al., 2023), aiming to adapt it for continuous turbidity monitoring in aquatic environments, while also enabling the differentiation between turbidity caused by algae and that caused by inorganic particles. The initial design concept and physical assembly of the probe occurred prior to the scope of this research.

## 1.1 Research Questions and Hypothesis

**RESEARCH QUESTION** Can the low-cost turbidity sensor accurately distinguish between different sources of turbidity while maintaining acceptable measurement precision?

HYPOTHESIS 1: The sensor can effectively distinguish between different sources of turbidity, while maintaining mean absolute errors below 5 NTU.

HYPOTHESIS 2: The sensor demonstrates high performance in laboratory conditions but loses accuracy and classification ability under continuous monitoring scenarios.

## 1.2 General Objective

The general objective of this work is to evaluate a low-cost optical prototype for turbidity measurement, with the potential for continuous monitoring and the identification of algae-related turbidity.

## 1.3 Specific Objectives

- Calibrate the prototype, establishing the calibration curves and corresponding mathematical models;
- Evaluate the prototype's ability to distinguish between different sources of turbidity under controlled laboratory conditions;
- Assess the performance and stability of the prototype during continuous monitoring experiments in the laboratory;
- Propose improvements to the probe's design based on the results obtained throughout the experimental stages.

# 2 Literature Review

This chapter presents a literature review aimed at defining turbidity and its relationship with overall water quality, including its indirect effects on potability and implications for water treatment. It also explores how turbidity is connected to phenomena such as eutrophication, resuspension in aquatic systems, and industrial discharges in urban environments. Additionally, relevant national and state legislation concerning water quality (particularly those that include turbidity as a monitored parameter) is reviewed. Finally, five key studies from 2014 onward (KELLEY et al., 2014; PARRA et al., 2018; GILLETT; MARCHIORI, 2019; ROCHER et al., 2021; DROUJKO; MOLNAR, 2021) are analyzed to assess the state of the art in low-cost turbidity sensor development.

## 2.1 Water quality

### 2.1.1 Water quality

Water is a fundamental resource for human health, ecosystems, and socioeconomic development, with variations in its quality affecting all these aspects significantly. For instance, variations in the water quality in rivers and lakes environments can result in changes in the quality of recreational and commercial activities (ADJOVU et al., 2023) as well as potentially exceeding ecosystem tolerance thresholds and leading to degradation (MURDOCH; BARON; MILLER, 2000). Water quality also impacts water treatment processes and costs, with poor source water quality demanding additional treatment processes and operational adjustments, resulting in increased energy use and higher expenses (SANTANA; ZHANG; MIHELCIC, 2014). Moreover, over 50 diseases are known to be caused by unsafe drinking water, and globally, 80% of all diseases and 50% of child deaths are associated with poor water quality (LIN; YANG; XU, 2022)

In this context, water quality monitoring is crucial for ensuring safe drinking water, effective water treatment, preserving aquatic ecosystems (KLIMASZYK; GOŁDYN, 2020), and overall public health protection (KEELER et al., 2012). Key parameters utilized for this monitoring include physical (e.g., turbidity, temperature, electrical conductivity), chemical (e.g., pH, dissolved oxygen, nutrients, heavy metals), and biological (e.g., algae and pathogens concentration) factors.

Drinking water is defined as water that does not pose a significant health risk over a lifetime of consumption, including sensitivities that may occur across different life stages (World Health Organization, 2017a), and it is recognized as an essential and inalienable human right (United Nations, 1948). However, despite international efforts to universalize access to this resource and ensure its availability to all populations, regardless of geographic location or socioeconomic status (United Nations, 2015), there are no internationally standardized criteria for drinking water quality, leaving each country responsible for establishing its own regulatory frameworks and specific legislation.

In Brazil, the National Water Agency (ANA) was established in 2000 by Law No. 9,984/2000. ANA acts as a regulatory agency tasked with implementing the objectives and guidelines of Law No. 9,433/1997, which established the National Policy of Water Resources, and Law No. 14,026/2020, which updated the legal framework for basic sanitation.

One of ANA's lines of action is the monitoring of water quality, which involves obtaining quan-

Table 1 – Water quality categories based on the WQI range.

| Category | Range |
|---|---|
| **Excelent** | $79 < \text{WQI} \leq 100$ |
| **Good** | $51 < \text{WQI} \leq 79$ |
| **Medium** | $36 < \text{WQI} \leq 51$ |
| **Bad** | $19 < \text{WQI} \leq 36$ |
| **Very bad** | $\text{WQI} \leq 19$ |

Table 2 – Parameters relative weight used in the calculation of the WQI

| Parameter | Relative weight ($w_i$) |
|---|---|
| Dissolved oxygen | 0.17 |
| Thermotolerant coliforms | 0.15 |
| pH | 0.12 |
| BOD | 0.10 |
| Water temperature | 0.10 |
| Total nitrogen | 0.10 |
| Total phosphorus | 0.10 |
| Turbidity | 0.08 |
| Total solids | 0.08 |

titative information on indicators and parameters that are representative of the physical, chemical, and biological characteristics of the water in specific reaches of a water body over a period of time. This allows for the detection of environmental changes and the assessment of the status and quality of national water resources. Water quality monitoring is also utilized to support management, licensing, and oversight actions in river basins and other water bodies, as well as to evaluate compliance with current environmental legislation.

### 2.1.2 Water Quality Index (WQI)

The Water Quality Index (WQI, or in portuguese "*Índice de Qualidade das Águas*") is currently the main qualitative indicator used in Brazil. It is based on a methodology originally developed in 1970 by the U.S. National Sanitation Foundation and later adapted by CETESB (Companhia Ambiental do Estado de São Paulo). The index incorporates nine physical, chemical, and biological parameters: water temperature, pH, dissolved oxygen, biochemical oxygen demand (BOD), thermotolerant coliforms, total nitrogen, total phosphorus, total solids, and turbidity. This enables the simultaneous evaluation of multiple variables considered essential for assessing water quality, providing a single value ranging from zero to one hundred, which facilitates interpretation and comparison. These values are subsequently grouped into defined water quality categories (Table 1)

For each parameter, relative weights (Table 2) and quality rating curves (Figure 1) were defined according to the status or conditions of each of the nine parameters. Based on these criteria, the WQI is calculated using a weighted geometric mean of the water quality values corresponding to the variables that comprise the index, as described by the equation below:

$$IQA = \prod_{i=1}^{n} q_i^{w_i}, \tag{2.1}$$

where $q_i$ is the quality rating of the $i$-th parameter, a number that varies from 0 to 100, depending on the respective quality variation curve based on its concentration or measurement. $w_i$ is the weight assigned to the $i$-th parameter, varying between 0 and 1 based on its importance to the overall water quality assessment.

Figure 1 – Quality variation curve for turbidity utilized in the WQI calculation, based on its concentration or measurement. $q_s$ is the quality rating for a determined turbidity value. Source: Instituto Mineiro de Gestão das Águas (IGAM) ().

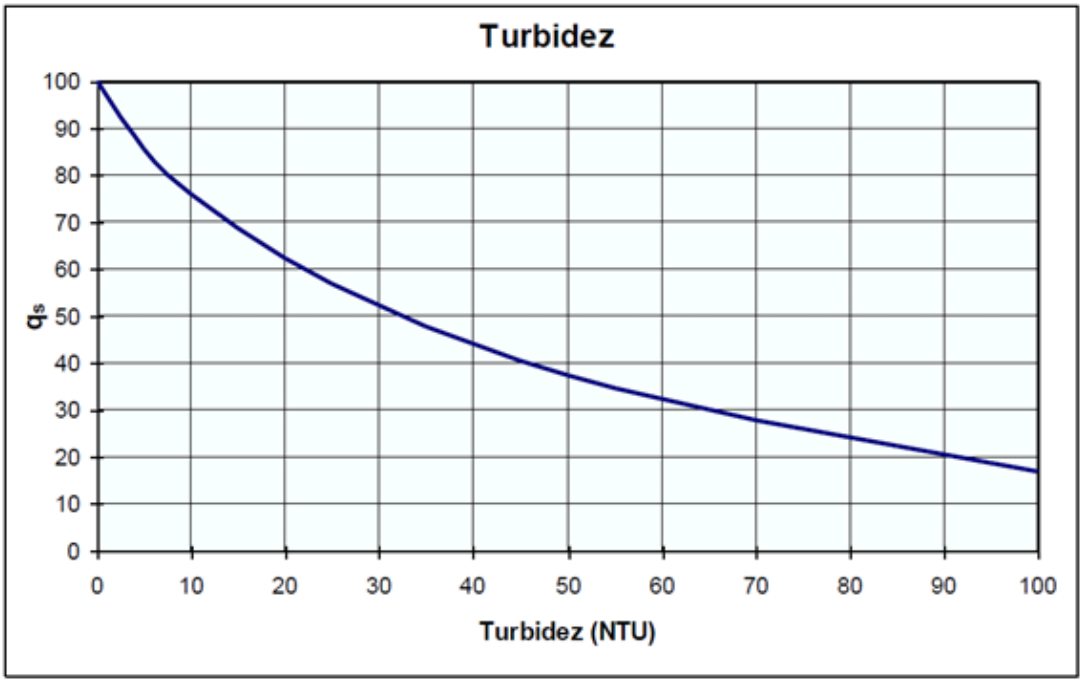


Turbidity is, therefore, one of the key parameters for assessing water quality, with a weight of 0.08 (8%) in the WQI calculation. Its quality rating curve is approximately exponential, with water quality declining as turbidity increases. This reinforces turbidity's importance as both a diagnostic and regulatory parameter for environmental and public health protection.

## 2.2 Eutrophication

Aquatic ecosystems are often classified based on their nutritional status. Nutrient-poor water bodies with low primary productivity are referred to as oligotrophic, while nutrient-rich waters with high productivity are called eutrophic. The trophic status of a lake is determined by natural processes related to climate, morphology, and size (BOWMAN; HACKER; CAIN, 2017), with lakes naturally tending to evolve from oligotrophic to eutrophic over time, in a process known as eutrophication.

Human activities significantly impact the biogeochemical cycles of elements such as nitrogen (N) and phosphorus (P) (VITOUSEK et al., 1997; VUILLEUMIER et al., 2021), thereby accelerating eutrophication in many water bodies through sewage discharge, agricultural fertilizers, and industrial waste containing elevated concentrations of these nutrients. These elements directly influence the growth and proliferation of algae and phytoplankton in freshwater and marine ecosystems (HECKY et al., 1988), acting as limiting factors for Net Primary Production (NPP), which is defined as the energy captured via photosynthesis minus the energy lost through cellular respiration. Suspended sediments in rivers can limit light penetration; thus, turbidity can also directly influence and regulate NPP (BOWMAN; HACKER; CAIN, 2017).

The intensification of eutrophication processes can degrade water bodies, potentially leading to the loss of key species and important ecosystem services (CARPENTER et al., 1998). In such cases, turbidity plays an important role, serving as an indicator of nutrient levels. As a consequence, the eu-

trophication status of a water body can be correlated with planktonic or algal density in the water column (BOWMAN; HACKER; CAIN, 2017).

## 2.3 Turbidity

### 2.3.1 Definition

Turbidity is a parameter that represents water opacity due to suspended particles, quantified by the attenuation and scattering of electromagnetic radiation (e.g., visible light, infrared) passing through a fluid. The presence of dispersed particles can be indirectly measured via the optical interactions between suspended material and incident light (SADAR, 2003). In a pure water system, light rays travel in a straight path, although even water molecules scatter some light, producing a baseline turbidity. When suspended solids are present, light scattering depends on the chemical and geometric properties of the particles and the wavelength of the radiation. Changes in water transparency can affect aquatic ecosystems parameters like pH, temperature, and dissolved oxygen levels (AZIS et al., 2015).

Turbidity may increase due to the presence of both organic (e.g., microalgae and bacteria) and inorganic (e.g., silica and clay) particles. Elevated levels of suspended solids pose potential concerns for water quality, with recent studies linking increased turbidity to higher risks of gastrointestinal infections (World Health Organization, 2017b). Turbidity may also serve as an indicator of eutrophication and the presence of pathogens or contaminants that can adhere to particulate matter (VUILLEUMIER et al., 2021), reducing the effectiveness of different water treatment stages like filtration (MONTOYA-PACHONGO et al., ) and disinfection by UV (CHRISTENSEN; LINDEN, 2003; GULLIAN et al., 2012) or by chlorination (LECHEVALLIER; EVANS; SEIDLER, 1981), also affecting the detection of coliforms in water samples (LECHEVALLIER; EVANS; SEIDLER, 1981) and overall, affecting domestic, industrial, and recreational uses of water (DROUJKO; MOLNAR, 2021; SANTOS, 2022). Algal blooms can increase turbidity (FISCHER; FROMMEN, 2013), which poses different ecological and water quality implications than turbidity from other sources. By identifying the origin of suspended particles, it is possible to infer the eutrophication status of a water body through turbidity measurements (ROCHER et al., 2021).

In urban areas, turbidity increases often result from domestic and industrial discharges, frequently associated with drainage infrastructure and non-point source pollution. In rural areas, irregular occupation of protected zones (e.g., Permanent Preservation Areas) may contribute to increased turbidity. Suspended solids may also be resuspended during rainfall events (BLOESCH, 1994).

Thus, turbidity is an extremely useful indicator for detecting and assessing suspended solids, erosion processes in watersheds, pollution sources, eutrophication, and related phenomena. It provides valuable information about water quality in a rapid, relatively inexpensive, and continuous manner, applicable across a wide range of systems, from artesian wells to advanced water treatment facilities (World Health Organization, 2017b).

### 2.3.2 Measurement methods

Initially, turbidity was measured through visual inspection using optical principles, specially relating it to the depth at which a standardized object becomes obscured underwater. Instruments like the Turbidity Tube (Figure 2a) and Secchi Disk (Figure 2b) were developed based on this principle, measuring the depth at which a bicolored object is no longer visible (FALCADE; MANNICH; COLOMBO, 2017).

Figure 2 – Different measurement methods for turbidity. a) Turbidity disk. Source: (FALCADE; MANNICH; COLOMBO, 2017). b) Secchi disk.

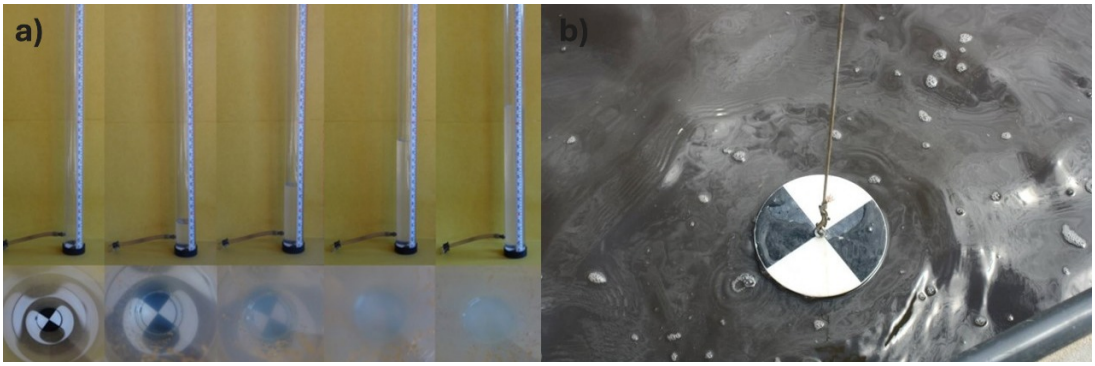


Subsequently, with technological advances, electronic devices were developed, including nephelometers and digital bench turbidimeters, both of which require trained professionals for sample collection and measurement. These devices typically consist of an infrared light source and a detector.

The main distinction between turbidimeters and nephelometers lies in the position of the sensor relative to the light source. In turbidimeters, the sensor is placed opposite the light source, measuring the transmitted light intensity. In contrast, nephelometers position the sensor at a 90° angle, measuring scattered light. In nephelometric methods, greater light scattering correlates with higher turbidity levels (BUENO et al., 2023). Turbidity is commonly expressed in Nephelometric Turbidity Units (NTU), although other units may also be used (World Health Organization, 2017b).

#### 2.3.2.1 State of art

Given the essential role of turbidity in water quality assessment, serving as a proxy for erosion, sediment transport, eutrophication, and pollution events, there is an increasing demand for efficient, continuous, and field-deployable sensing technologies. While traditional laboratory analyses provide high accuracy, they are often logistically impractical for real-time decision-making and inaccessible in remote or low-income regions. Commercial turbidimeters, though reliable, are frequently cost-prohibitive and rarely adaptable to measure additional indicators, and are incapable of determining the origin of turbidity. These limitations have driven recent efforts toward the development of low-cost, open-source sensors capable of measuring turbidity with reasonable accuracy and affordability.

In this context, this section presents a review of key studies that address this technological gap, by proposing and developing low-cost turbidity sensors that utilize LED light sources and electromagnetic radiation detectors (DROUJKO; MOLNAR, 2021; GILLETT; MARCHIORI, 2019; KELLEY et al., 2014; ROCHER et al., 2021; PARRA et al., 2018). Since these sensors operate via electrical signals, their output (e.g., in volts, ohms, or hertz) can be calibrated and correlated to standard turbidity units such as $NTU$.

Droujko and Molnar (2021) proposed three versions (A, B, and C) of a low-cost turbidity sensor designed for in situ measurement of suspended sediment concentration (SSC) in alpine river networks. Each version operates with an 850 nm infrared LED and two optical detectors (TSL237S-LF) positioned at different angles (90°, 135°, or 45°, depending on the version), allowing the measurement of scattered light. For calibration, solutions were prepared with two types of sediments: feldspar and sediments collected from the Fieschertal channel in Switzerland. The adopted technique uses the difference between the readings of the optical detectors with the LED turned on and off to mitigate ambient light interference. These values (in Hertz) were directly converted to SSC ($g/L$) using an equation obtained during calibration. The prototype showed relative errors of less than $\pm 10\%$ for raw measurements and less than $\pm 5\%$ for processed

values, with $R^2$ values greater than 0.98, considering direct calibration for SSC over a sampling range of 0 to 16 g/l (approximately 0 to 4000 NTU. The three versions were compared to three commercial models, demonstrating better performance, especially at low concentrations. The models had an average assembly cost of 61.37 Swiss francs (CHF) equivalent to approximately US$ 74.65 (as of June of 2025). Versions A and B were built with PVC, while version C was fabricated using 3D printing. The sensor uses an ESP32 microcontroller, which, despite having Wi-Fi and Bluetooth connectivity, was used only for data acquisition in the study, without remote transmission. The article did not aim to identify or distinguish the source of turbidity or suspended sediments and suggested future steps such as the integration of temperature and pressure sensors and the implementation of an automatic wiper.

Kelley et al. (2014) proposed a sensor that uses the nephelometric principle with an 860 nm infrared LED and a light-to-frequency sensor (TSL230R) that measures pulse frequency proportional to scattered light. The sensor was designed for drinking water monitoring in low-income communities or remote areas, particularly to detect turbidity spikes caused by events such as sediment runoff during storms. The sensor uses an ATMega328P-PU Arduino microcontroller, powered by four AA batteries, with a battery life of up to 3 months under hourly samplings conditions. The total cost of the prototype ranges from US$ 25 to 35. For calibration, 25 solutions of hydrophilic oil diluted in distilled water were prepared, with turbidity values ranging from approximately 0.01 to 1100 NTU. Four linear regressions were defined for different turbidity ranges (0–0.5, 0.5–30, 30–300, 300–1000 NTU), allowing the conversion of measured frequency ($Hz$) to turbidity values ($NTU$). The regressions closely matched observed values, with $R^2 \geq 0.9990$ for turbidity $> 0.5$ NTU and $R^2 \geq 0.9977$ for turbidity $< 0.5$ NTU. The prototype's turbidity values were compared to those from a commercial sensor, with 192 out of 200 measurements (96%) falling within $\pm$ 3% or $\pm$ 0.3 NTU (which was greater) of the commercial device's average measurement for each calibration solution. Additionally, five non-formazin turbidity standards (0.02, 1, 10, 100, and 1000 NTU) were used to evaluate the prototype's precision, yielding RMSE (root mean squared error) values of 0.02, 0.08, 0.33, 9.54, and 31.5 NTU, respectively. Open-source turbidimeter versions were also designed with an integrated GSM modem, enabling communication with a web server via Wi-Fi (GPRS) and cellular network (GSM).

Parra et al. (2018) proposed an optical sensor based on the Beer-Lambert law, using LEDs of different wavelengths (infrared, green, yellow, and red) and two detectors positioned at 180° (a light-dependent resistor for visible light and a photodiode for infrared). The prototype has an approximate cost of €8.30 (excluding the microcontroller and housing), or approximately US$ 9.46. The sensor was designed for water quality monitoring in aquaculture farms, particularly in saline or coastal environments. For calibration, three turbidity sources were used: river sediments (composed primarly of silt, clay, and sand) and two algae species (Isochrysis galbana and Tetraselmis chui). Turbidity (NTU) was estimated from the variation in sensor resistance ($\Omega$) using exponential regression models, with distinct models for each LED-turbidity source combination. The best results were obtained with infrared and red LEDs, which had $R^2$ values of 0.994 and 0.999, respectively. The infrared LED was selected for turbidity quantification, while the red LED was used to identify the turbidity source, successfully distinguishing between sources at turbidity levels $> 12$ NTU. During verification (using red light), the sensor exhibited a mean absolute error of 0.65 NTU and a relative error of  3%. Future work includes expanding the analysis to additional phytoplankton species and developing a wireless sensor network (WSN) integrating the turbidity sensor with other water quality sensors.

Rocher et al. (2021) developed a low-cost optical absorption sensor for quantifying algae concentration in irrigation reservoirs. The sensor operates on the turbidimetric principle and incorporates six LEDs (blue, green, yellow, orange, red, and infrared) paired with six detectors (five LDRs for visible light and one photodiode for infrared detection). For calibration, two turbidity sources were used: sediments

and algae (Chlorella vulgaris). Seven solutions were prepared, including two pure samples and five mixed samples with varying ratios of each turbidity source. Tap water was used for dilution, yielding eight concentrations per solution type. The resistance variations ($\Omega$) from each LDR were converted to voltage ($V$). Seven linear regressions were established for different solid concentrations (15, 50, 200, 500, 800, 1500, and 4000 mg/L), enabling voltage (V) to algae concentration (mg/L) conversion. The combined model achieved an average error of 36.52 mg/L (12.56% relative error) between predicted and observed concentrations. The prototype first uses the infrared LED to determine the total solids concentration, then applies the nearest regression equations for algae concentration interpolation. The study also explored an artificial neural network (ANN) to estimate algae percentage in mixed samples. While the ANN outperformed the proposed algorithm (achieving 100% classification accuracy during validation), it demanded significantly greater computational resources and energy. Regarding telemetry, the authors proposed a hybrid Wi-Fi/LoRa communication system, though this concept was not implemented or evaluated in the study and remains a suggestion for future applications.

Gillett and Marchiori (2019) developed a low-cost nephelometric sensor for continuous water quality monitoring, featuring a white LED and a light sensor paired with an ESP32 Wi-Fi microcontroller. The prototype was constructed at an approximate cost of US$ 64. For calibration, four identical low-cost continuous turbidity sensors were evaluated across a turbidity range from 0.02 to 100 NTU. Test solutions were prepared by diluting a 4000 NTU formazin standard solution with deionized water to achieve 0.20, 5, 20, 40, and 100 NTU standards. Output frequency values ($Hz$) were converted to turbidity ($NTU$) using a derived calibration equation and validated against a commercial turbidimeter. The prototype achieved $\pm 1$ NTU measurement reliability, though some signal noise was observed. A large-scale laboratory test was conducted using a 3785 liters (1000-gallon) water tank and 1000 GPH pool pump. Sensors were installed at both the pump inlet and outlet, with Wi-Fi-transmitted data stored in a database. During 38 days of continuous monitoring (including induced turbidity changes using coffee powder), the sensor demonstrated a median residual and standard deviation for inlet and outlet of - 0.4507 and 1.9063 NTU, and 1.3997 and 6.5511 NTU, respectively. While responsive to turbidity variations, field performance showed reduced accuracy ( $\approx 5$ NTU) compared to controlled lab tests. The main sources of error were air bubbles in plumbing (particularly affecting the outlet sensor) and ambient light interference.

Table 3 presents a comparison between the low cost sensors proposed in these articles, considering aspects such as: what are the parameters analyzed, the adopted angle between the LEDs and sensors, the estimated costs, the ability to distinguish between the turbidity origin and if the sensors have a wiper system implemented.

Table 3 – Comparison between low cost sensors proposed in different articles.

| **Category** | **Kelley et al. (2014)** | **Parra et al. (2018)** | **Gillett and Marchiori (2019)** | **Rocher et al. (2021)** | **Droujko and Molnar (2021)** |
|---|---|---|---|---|---|
| Analysis parameters | Frequency ($Hz$) → Turbidity ($NTU$) | Resistance variation (Ohms) → Turbidity ($NTU$) | Frequency ($Hz$) → Turbidity ($NTU$) | Resistance variation (Ohms) → Voltage ($V$) → Algae concentration ($mg/L$) | Frequency ($Hz$) → Suspended sediment concentration SSC ($g/L$) |
| Analysis range | 0–1100 NTU | 0–200 NTU | 0.02–100 NTU | 15–4000 mg/l | 0–16 g/l SSC (approximately 0–4000 NTU) |
| Emission | 1 infrared LED | 1 infrared LED and 3 visible light LEDs (red, yellow and green) | 1 visible light LED (white) | 1 infrared LED and 5 visible light LEDs (blue, green, yellow, orange and red) | 1 infrared LED |
| Detection | 1 light-to-frequency converter | 1 photodiode (IR) and 1 LDR (visible light) | 1 ambient light sensor | 1 photodiode (IR) and 5 LDRs (visible light) | 2 light-to-frequency converters |
| Angle between LEDs and sensors | 90° | 180° | 90° | 180° | 45°, 90° and/or 135° |
| Application | Drinking water monitoring in low-income communities or remote areas | Water quality monitoring in aquaculture farms, particularly in saline or coastal water systems | Continuous water quality monitoring | Algae concentration monitoring in irrigation reservoirs | SSC monitoring on alpine river networks |

| **Category** | **Kelley et al. (2014)** | **Parra et al. (2018)** | **Gillett and Marchiori (2019)** | **Rocher et al. (2021)** | **Droujko and Molnar (2021)** |
|---|---|---|---|---|---|
| Solutions used for calibration or validation | 1 type (calibration): Hydrophilic oil diluted in distilled water and 1 type (validation): non-formazin turbidity standards | 3 types (calibration): River sediments (composed mainly of silt, clay, and sand) and two algae species (Isochrysis galbana and Tetraselmis chui) | 1 type (calibration): Formazin standard (4000 NTU) diluted in deionized water and 1 type (continuous monitoring experiment): coffee powder | 2 types (calibration): Sediments and algae (Chlorella vulgaris) | 2 types (calibration): Sediments (feldspar and sediments collected from the Fieschertal channel) |
| Adopted mathematical models | 4 linear regressions for distinct ranges | Exponential regression | Ordinary least squares linear regression | 7 Multiple regression models and neural network | Fourth order multiple linear regression |

| **Category** | **Kelley et al. (2014)** | **Parra et al. (2018)** | **Gillett and Marchiori (2019)** | **Rocher et al. (2021)** | **Droujko and Molnar (2021)** |
|---|---|---|---|---|---|
| Precision/ Accuracy | $R^2 > 0.9990$ (for turbidity $> 0.5$ NTU) and $R^2 = 0.9977$ ( for turbidity $< 0.5$ NTU), 192 out of 200 prototype measurements (96%) fall within 3% or 0.3 NTU (whichever is greater) of the average measurement obtained by the commercial turbidimeter and RMSE values of: 0.02, 0.08, 0.33, 9.54, and 31.5 NTU for non-formazin turbidity standards of: 0.02, 1, 10, 100, and 1000 NTU, respectively. | for calibration: $R^2$ values of 0.994 (infrared emission) and 0.999 (red emission). And for validation: MAE up to 0.65 NTU and relative errors of 3% (red emission) | For calibration: Able to reliably estimate turbidity within 1 NTU, although some noise was present. And for the continuous monitoring experiment: median residual and standard deviation for the inlet and outlet sensors were - 0.4507, 1.9063 NTU and 1.3997, 6.5511 NTU, respectively. | Average error between predicted and observed algae concentration was 36.52 mg/l with a relative error of 12.56 % | Relative errors $<$ ś10% for raw measurements and $<$ $\pm$5% for processed values and $R^2 > 0.98$ |
| Estimated cost | US$ 25–35 | €8.30 (without microcontroller and casing) | US$ 64 | Not mentioned | 61.37 CHF |
| Telemetry | WiFi (GPRS) and cellular network (GSM) | Future work: Creation of a a wireless sensor network (WSN) | WiFi communication | Future work: WiFi and LoRa communication | Not implemented |

| Category | Kelley et al. (2014) | Parra et al. (2018) | Gillett and Marchiori (2019) | Rocher et al. (2021) | Droujko and Molnar (2021) |
|---|---|---|---|---|---|
| Wiper | Not mentioned | Not mentioned | Not mentioned | Not mentioned | Future work |
| Differentiation between turbidity sources | Not mentioned | Able to distinguish between the three sources for turbidity levels above 12 NTU | Not mentioned | Neural network and multiple regression models were used to estimate the concentration of alga | Not mentioned |

Table 4 – Turbidity standards for treated water after filtration disinfection, as defined by Annex XX of Consolidation Ordinance No. 5/17 of the Ministry of Health.

| Water Treatment | Maximum Permitted Value (MPV) |
|---|---|
| Disinfection (for groundwater) | 1.0 NTU in 95% of samples |
| Rapid filtration (complete treatment or direct filtration) | 0.5 NTU in 95% of samples |
| Slow filtration | 0.5 NTU in 95% of samples |

As shown in Table 3, the reviewed studies demonstrate the feasibility of low-cost turbidity sensing based on optical principles. However, some recurring limitations such as the focus solely on measuring turbidity intensity (in *NTU* or solids concentration), without evaluating the capability to identify the origin of the suspended particles, limit their environmental diagnostic power and overall applicability. Moreover, a wide variation in optical configurations, calibration approaches, and statistical methodologies indicates a lack of standardization, affecting replication and cross-comparison.

In summary, although significant progress has been made in developing low-cost turbidity sensors, a clear gap remains: most prototypes are limited to quantifying turbidity and do not provide information about the nature or origin of the suspended matter. Only a few attempts, such as Parra et al. (2018), have explored this direction, but their applicability was limited by operational constraints and narrow scope, as it was not tested under real-world continuous monitoring conditions. To address these shortcomings, the present study proposes the calibration and enhancement of a low-cost optical prototype that uses RGB LEDs and a TCS230 sensor to perform turbidity measurements using different spectrum, in order to enable not only continuous monitoring but also the discrimination between turbidity caused by algae and that caused by inorganic particles, offering this way an accessible and affordable tool for water quality assessment.

### 2.3.3 Legislation

Environmental criteria for classification and management of water bodies, as well as discharge limits for effluents, are defined under Resolution No. 357 of March 17, 2005, issued by CONAMA (National Environment Council). This resolution is applicable nationwide and establishes quality standards based on designated uses for freshwater and saltwater bodies. Among the parameters listed, turbidity must not exceed 40 NTU for freshwater bodies classified as Class 1 and 2, while the limit for Class 3 is set at 100 NTU.

In addition, the treated water supplied by SANEPAR (Companhia de Saneamento do Paraná) must comply with the potability standards defined in Annex XX of Consolidation Ordinance No. 5/17 of the Brazilian Ministry of Health. These standards were later updated by Ordinances GM/MS No. 888/2021 and No. 2.472/2021, which establish maximum turbidity limits for treated water after disinfection and filtration(Table 4).

# 3 Methods

This chapter provides a detailed description of the adopted prototype and outlines the main methodological steps developed to enhance its performance (Figure 3). The initial development and physical assembly of the probe were completed prior to the scope of this research.

Figure 3 – Study steps flowchart

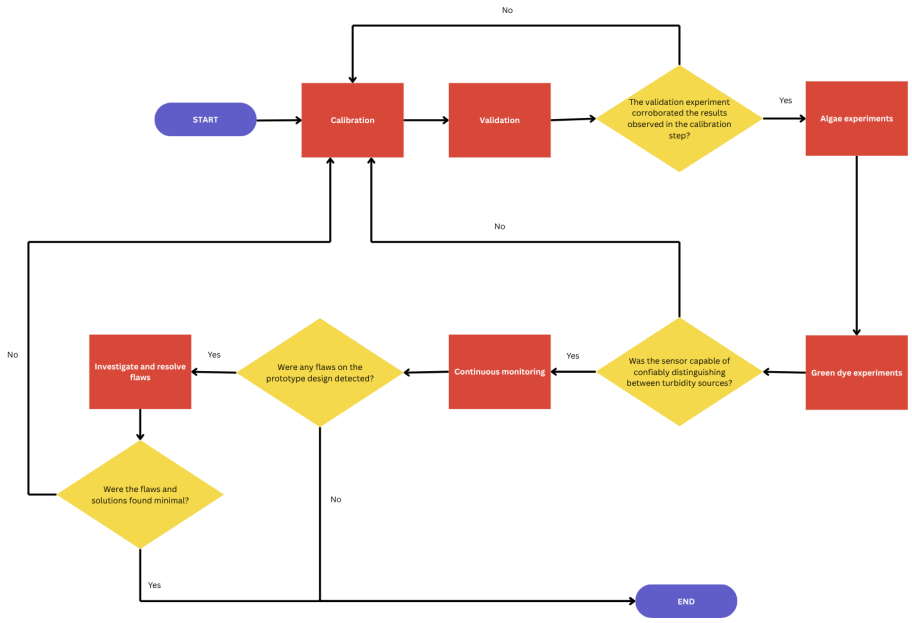


The initial stages focused on the calibration and validation of the prototype to assess its ability to accurately measure turbidity. Validation was performed to confirm the results obtained during the calibration step. The subsequent step was to evaluate whether the prototype could differentiate between sources of turbidity, with emphasis on algae identification. For this purpose, two procedures were employed: experiments with real algae and with green dye. Posteriorly, further tests were conducted under continuous monitoring conditions to evaluate the system's stability and identify potential design limitations

## 3.1 Prototype description

The probe was built from a polyvinyl chloride (PVC) pipe with two perforated ends, allowing water to pass through the probe's interior in the measurement area. At each end, a layer of perforated rubber helps create a maze-like layout, in order to reduce the effects of sunlight (external light) on the sensor readings (Figure 4). The internal configuration of the prototype is based on the nephelometric principle for turbidity measurement, with an RGB light-emitting diode (RGB-LED) positioned perpendicularly to a TCS230 sensor, which contains a total of 64 photodiodes that quantify and convert the intensity of electromagnetic radiation into a digital electrical signal interpreted by the microcontroller (BUENO et al., 2023). The RGB LED was configured to intermittently emit electromagnetic radiation at wavelengths corresponding to the colors white, green, and red during the measurement process.

The TCS230 sensor is capable of differentiating the intensity of different wavelengths, identifying the emitted colors. For this study, three intensities were programmed on the Arduino board to be read

Figure 4 – Probe's layout. a) Representation of the maze-like structure in both extrimities of the sensor. The dashed black lines represents the holes that allow water to reach and exit the probe's interior (monitoring area). b) Representation of the probe's interior, indicating the nephelometric positioning of the detector (TCS230).

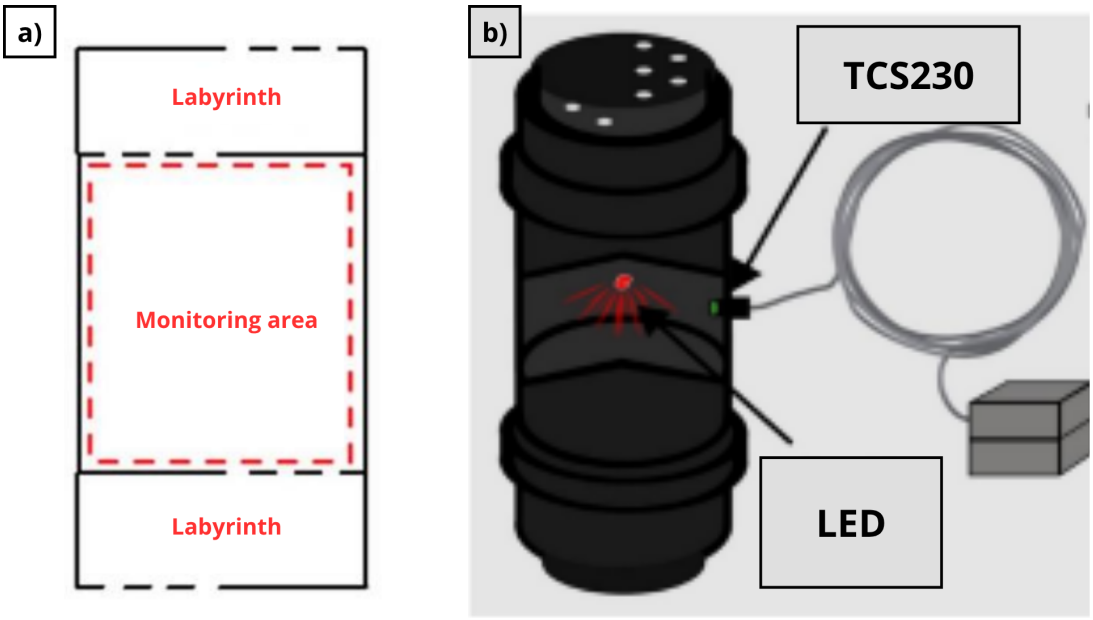


by the sensor (red, green, and unfiltered). For data acquisition, one color at a time was emitted by the RGB LED, with eight measurements being performed simultaneously in the three intensities read by the photodiode, at approximately two-second intervals. A complete cycle (considering the emission of the three colors) takes approximately 48 seconds. Data storage was performed on an SD card inserted into the Data Logger.

The output data from the TCS230 sensor is a frequency value (Hz) related to the intensity of the received light (identified by the sensor for the given wavelength, among red, green, and white). The developed prototype operates on principles similar to those used by de Bueno et al. (2023) and Droujko and Molnar (2021), except that the one previously developed by Bueno et al. (2023), which used an analog light-dependent resistor (LDR) sensor limited by the 10-bit resolution of the microcontroller. Droujko and Molnar (2021) used a sensor similar to the TCS230, but without the ability to distinguish the intensity of different wavelengths, as it consisted of only one photodiode sensor without a filter.

An Arduino Nano board with an Atmega328p microcontroller was used for data control and acquisition. A Data Logger shield model data logging board ID:8122 Deek-Robot was responsible for data acquisition. This peripheral can maintain accurate sampling time tracking due to a Real Time Clock (RTC) integrated into the board. Initially, the system was powered via a USB connection (5 V) from an external computer, but can be powered by 12 V batteries to a autonomy application.

The electronic circuit was assembled on a PCB board, which was installed in a 6.5x10x8 cm box that serves as a control station (Figure 5), containing the Data Logger, the USB cable, the battery cables, as well as the wiring for the RGB LED and TCS230 sensor.

## 3.2 Prototype calibration

Initially, the probe's interior was completely filled with tap water (2500 ml). For the calibration of the prototype, successive additions of turbidimetric mixture containing formazin (4000 NTU) were

Figure 5 – Prototype developed for turbidity measurement. The monitoring station houses the detector and LED, while the control station contain the micro controller and the DataLogger, responsible for the control and acquisition of the data.

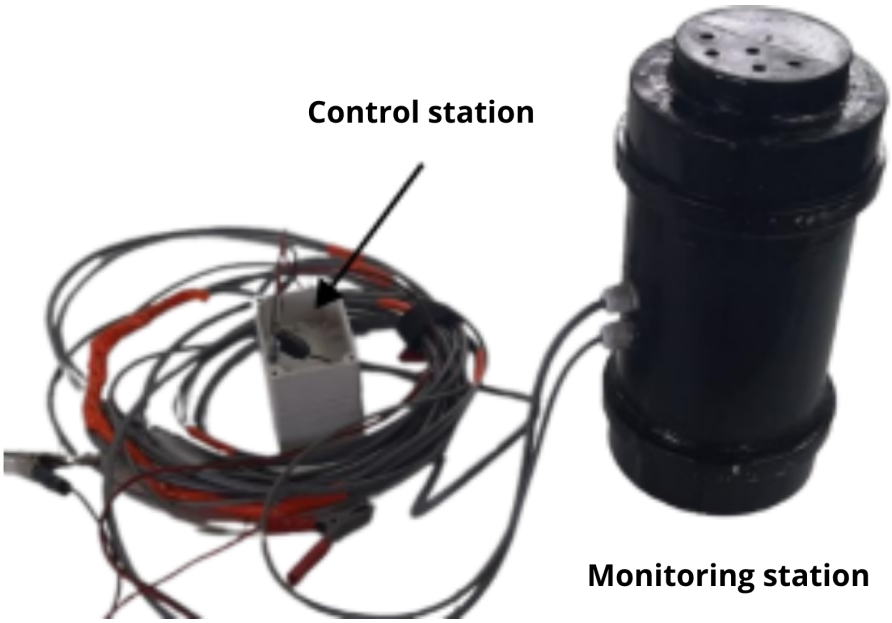


performed within the device gradually increase the water turbidity.

Two sets of experiments were conducted during calibration covering a total range of 0-200 NTU. In the first set, encompassing the range 0-80 NTU, the turbidimetric solution was prepared by diluting 50 ml of 4000 NTU formazin solution in 1000 ml of water, yielding a turbidity of approximately 292.25 NTU. The gradual increase in turbidity was achieved in each step of the experiment by adding 30 ml of the solution, representing an average increase of approximately 2.906 NTU per step. Throughout the second set of experiments, that covered the total range, the turbidimetric solution was prepared by diluting 150 ml of 4000 NTU formazin solution in 1000 ml of water, resulting in a turbidity of approximately 863.5 NTU. For each step during these experiments, the same volume of the prepared solution was added inside the probe, representing a mean increase of nearly 8.613 NTU per step.

For each injection of turbidimetric solution, an equal volume of water was removed from the probe to maintain a constant internal volume. Following each addition, the sensor recorded measurements for approximately 6 minutes, encompassing more than 6 complete cycles for each emitted and detected light configuration. During post-processing, the first three minutes of each round were considered a stabilization interval for the water within the monitoring area; measurements obtained during this period were discarded, and only the data acquired in the subsequent three minutes were used for analysis and results.

During each step, following the 6 minutes measurement interval, a sample was extracted from the prototype using a syringe to determine turbidity with a DLT-WV benchtop turbidimeter, which served as the reference for prototype calibration. The DLT-WV turbidimeter has a measurement range of 0.00 to 1000 NTU, with a resolution of 0.01 NTU up to 9.99 NTU, 0.1 NTU up to 99.9 NTU, and 1 NTU from 100 to 1000 NTU, with automatic range selection. The device detects particles larger than 0.1 µm and has an accuracy of ±2% F.S. (full scale) from 0.01 to 9.99 NTU, ±2% F.S. from 10.0 to 99.9 NTU, and ±3% F.S. from 100 to 1000 NTU.

A total of 6 experiments were conducted on different days (four comprising the experiments described for the first set and two for the second one), with each experiment comprising 19 steps involving

the addition of 30 ml of the turbidimetric solution. During these tests, the turbidity inside the probe ranged from approximately 0 NTU (tap water) to 55.9 NTU for the first set and from 0 NTU to 166 NTU for the second one.

The data acquired from these tests were utilized to determine the calibration curves that described the relationship between the turbidity inside the probe (as measured by the digital sensor) and the frequency values measured by the light-to-frequency converter. The calibration curves were determined for each light emission-reception pair.

### 3.2.1 Prototype validation

For validation, two more experiments were conducted for different turbidity ranges (0-80 NTU and 80-200 NTU). For these experiments, the turbidimetric solutions presented a turbidity of 293 NTU and 763 NTU, with every step representing an average increase of about 2.882 NTU and 8.049 NTU, respectively, covering the same turbidity range as the calibration phase.

### 3.2.2 Statistical evaluation

To evaluate the calibration curves and compare them with the validation data, five statistical metrics were used: coefficient of determination ($R^2$), mean absolute percentage error ($MAPE$), root mean square error ($RMSE$), mean absolute error ($MAE$) and standard deviation ($\sigma$). These are defined as follows:

$$R^2 = 1 - \frac{SS_{\text{res}}}{SS_{\text{tot}}} \tag{3.1}$$

where $SS_{\text{res}}$ is the residual sum of squares and $SS_{\text{tot}}$ is the total sum of squares. $R^2$ can vary between 0 and 1, and provides a measure of how well observed values are replicated by the calibration curves. Values closer to 1 indicate a better fit, and represent that the model explains the observed data well.

$$MAPE = \frac{1}{n}\sum_{i=1}^{n}\left|\frac{y_i - \hat{y}_i}{y_i}\right|, \tag{3.2}$$

where $MAPE$ values can range from 0 to 1, being widely used for time series forecasting.

$$RMSE = \sqrt{\frac{1}{n}\sum_{i=1}^{n}(y_i - \hat{y}_i)^2} \tag{3.3}$$

$$MAE = \frac{1}{n}\sum_{i=1}^{n}|y_i - \hat{y}_i| \tag{3.4}$$

where $\hat{y}_i$ are the predicted values, $y_i$ are the observed values, and $n$ is the number of observations. Both $RMSE$ and $MAE$ are metrics that measure the error in the original target units (in this case, $NTU$). The RMSE is a measure of the dispersion of the residual values, which are in turn measurements of the distance between the regression curve and the data points, while $MAE$ is a measure of the error amplitude.

$$\sigma = \sqrt{\frac{\sum(x - \bar{x})^2}{n}} \tag{3.5}$$

where $x_i$ are the observed values of the sample, $\bar{x}$ is the mean value of these observations and $n$ is the size of the sample. The standard deviation ($\sigma$) quantify the variability of a dataset relative to its mean, whereas higher values reflect a wider dispersion across the range.

## 3.3 Algae experiments

To assess the prototype's effectiveness in detecting algae-induced turbidity, seven experiments using green algae were conducted. These experiments aimed to evaluate the best emission and detection combinations for measuring turbidity distinguishing between turbidity sources.

For these experiments the probe was initially filled with distinct solutions prepared by mixing different ratios of algae concentration and water. To calibrate the probe for detecting algae concentration, the total chlorophyll ($\mu$g/L) was measured by an AquaFlash Handheld Active Fluorometer that measures the total chlorophyll and photosynthetic efficiency using *in vivo* fluorescence detection. The sensor has a sensitivity of 0.3 $\mu$g/l of chlorophyll and a linear range of 0.3 – 100 $\mu$g/l. The prepared algae solutions presented concentrations of 12.65, 40.13, 49.07, 105.69, 133.12, 234.17, and 256.09 $\mu$g/l.

Figure 6 – Solutions with different concentrations prepared for the algae experiments.The total chlorophyll values were measured utilizing a digital fluorometer.

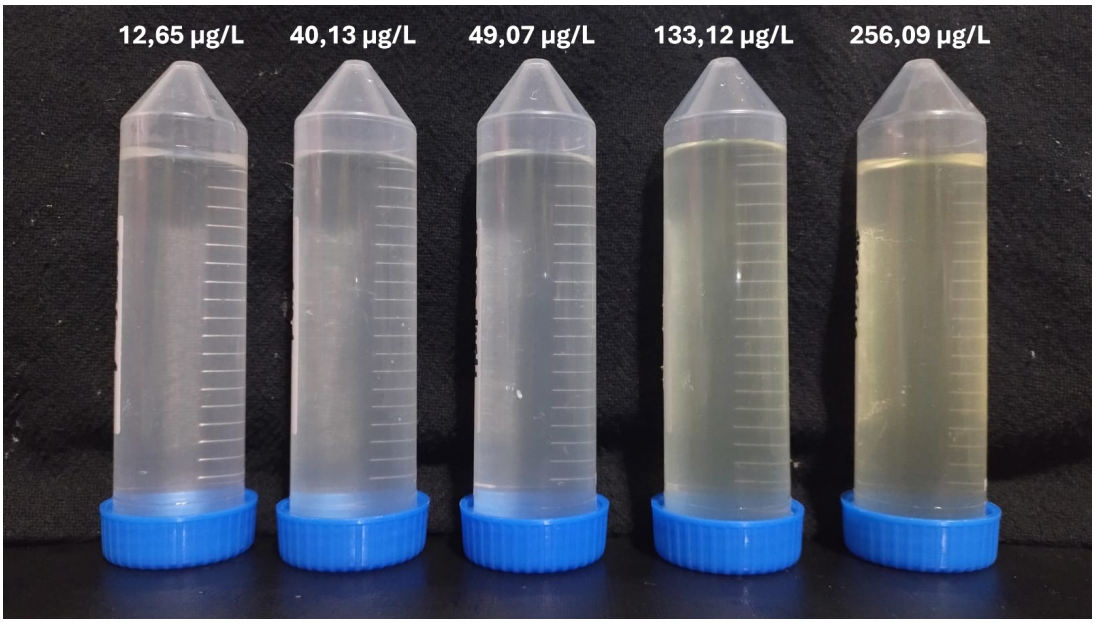


The experimental procedure followed the same procedure as the calibration and validation steps, with the preparation of the turbidimetric solution following the same procedure as described for the first set of experiments. During the tests, at each step, there was a mean increase of approximately 3.616 NTU, with the average turbidimetric solution turbidity being 294.80 NTU and the turbidity inside the probe fluctuating between 1.29 and 169 NTU throughout the experiments.

## 3.4 Green dye experiments

To compare results with those obtained from the formazin calibration experiments, as well as to evaluate whether green dye has the same response and can be used as an alternative to real algae during the probe calibration, additional tests were conducted using green food coloring.

For this series of experiments, the probe's interior was filled with solutions prepared by mixing 10 liters of tap water with different amounts of green dye. Four experiments were carried out, with the number of doses added being, chronologically: twenty, three, two, and one. Each dose corresponds to approximately 0.1 gram of dye, resulting in mean concentrations of 2.0, 0.3, 0.2, and 0.1 mg/l, respectively (Figure 7).

Figure 7 – Solutions with different concentrations prepared for the green dye experiments.

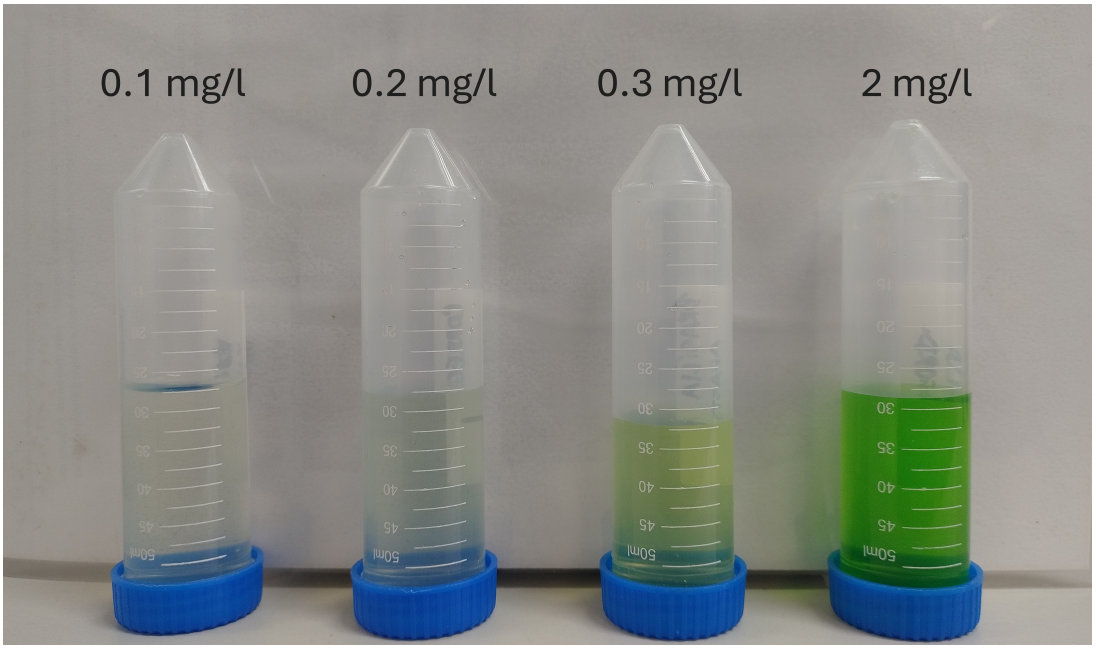


The experimental procedure followed the same protocol as the calibration and validation phases, except for the turbidimetric solutions and the volume added at each step. In this case, the solution was made by mixing 500 ml of tap water with 25 ml of the formazin solution, and at each step, 15 ml of this solution was added into the probe, corresponding to a turbidity increase of approximately 1.69 NTU. The turbidity range analyzed spanned from about 0 to 32.38 NTU, with the mean turbidity of the turbidimetric solution being 294.25 NTU.

## 3.5 Continuous monitoring tests

In order to evaluate the overall behavior of the probe for continuous monitoring, considering scenarios of turbidity increase and decrease, as well as to identify potential design flaws in the sensor, a recirculating system was assembled (Figure 8). Three experiments were conducted during this stage.

The system consisted of a 406 l tank, two buckets, hoses, a submersible pump, and the probe. The tank utilized had a parallelepiped geometry, having approximately 70 cm of width, 100 cm of length and 58 cm of height.

In order to create a flow through it, two buckets and hoses were utilized on opposite sides of the tank. One of the buckets was placed in a position above the water level, while the other was positioned at a lower one, in order to inject and remove, respectively, water or a turbidimetric solution into or from the tank, without the need for pumps.

Inside the tank, a submersible pump was positioned near the end of the hose connected to the bucket at the tank's inlet, in order to conduct water from the tank, to one of the probe's extremity.The probe was suspended horizontally at the tank center, slightly tilted above the water level, to allow drainage by gravity. The sensor was positioned so that the light-to-frequency converter was at the lower part of the probe.

At the beginning of each test, the tank was initially filled with clean water up to the height of 10 cm, which corresponded to a volume of approximately 70 l. The extremities of the hoses positioned

inside the tank, were fixated in the middle of the water column (approximately 5 cm). The outlet bucket was initially empty, while the inlet one was filled with a turbidimetric solution. Before the injection of any solution, the pump was turned on, and after the probe was completed filled, the DataLogger was turned on and the frequency data started to be recorded. At the beginning of the experiments, the system was kept running with only clean water for a few minutes, until any solution was added. Throughout the tests, as the inlet bucket containing the turbidimetric solution began to empty, it was filled with clean water, in order to gradually decrease the overall turbidity inside the tank, with this procedure being conducted up to four times, for each test.

During the experiments, the turbidity and eventually the total chlorophyll were measured multiple times using the digital sensors, in order to establish a background for comparison with the results obtained using the calibration curves. For these measurements, always a pair of water samples from the tank were taken, one from the area between the inlet hose and the pump, with it being representative of the water entering the sensor, while the other, was gathered from the water flowing out of the prototype. For subsequent analyses, the average of each pair of measurements was used.

For the first experiment, the turbidimetric solutions was prepared by mixing 10 liters of water with 400 ml of the 4000 NTU formazin solution, resulting in a turbidity of 211 NTU. The initial turbidity inside the tank was 0.05 NTU. The hose's extremity positioned at the bottom of the inlet bucket, was placed 60 cm higher than its other extremity (placed inside the tank), resulting in an average flow of 47 l/h or 0.000013 $m^3/s$. The outlet bucket was placed at a lower position in comparison with the tank, maintaining the same height difference between the hose's extremities.

For the second test, 800 ml of formazin and 20 liters of clean water were used for the solution, resulting in a turbidity of 180 NTU. The overall flow at the beginning of the experiment was also changed, reaching lower values close to $18,4$ l/h or 0.0000051 $m^3/s$, by using a height difference of 10cm. For the subsequent dilution stage, with the addition of clear water into the system, the adopted flow was the same as for the first experiment. Initially, the turbidity inside the tank was 0.06 NTU.

The third and final experiment aimed to evaluate the probe's behavior, considering the addition of a turbidimetric solution prepared by mixing tap water, formazin and algae. Initially, the solution was prepared by mixing only water and formazin, resulting in a turbidity of 170 NTU. At the beginning of the experiment, this turbidimetric solution containing only tap water and formazin began to be injected into the system, and when approximately half of it had been poured into the tank, 1000 ml of algae were mixed into the inlet's bucket, resulting in a new turbidimetric solution with a turbidity of 271 NTU and a total chlorophyll concentration of 585.67 $\mu$g/l. Throughout the entirety of the experiment, water samples from the probe's inlet and outlet were taken and measured for turbidity and total chlorophyll, using the digital sensors. The flow values presented during the second exeriment were adopted.

Figure 8 – Photos of the system assembled for the continuous experiments. a) System's overview. At the center, the probe suspended and slightly tilted. To the left,the inlet hose and bucket above the tank and the submerged pump. To the right, the outlet hose. b) Photo taken from the tank's "inlet" side, c)Photo taken from the tank's "outlet" side

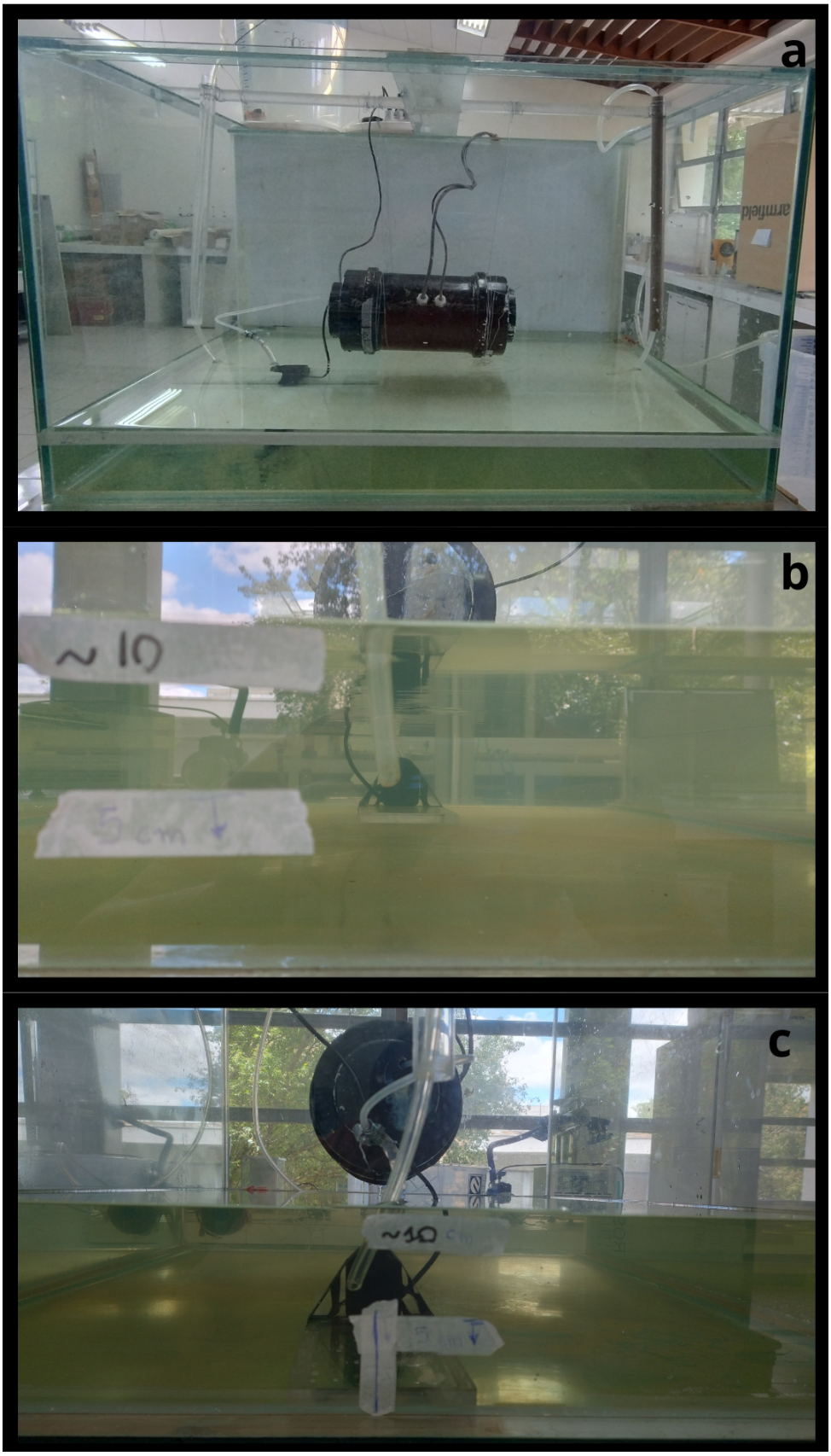

# 4 Results

## 4.1 Prototype operation

For each experiment, the volume of turbidimetric solution added to the system and the corresponding turbidity measured using the commercial turbidimeter were compared with the output frequency recorded by the TCS230 sensor for white, green, and red LED emissions. During each measurement step, the sensor acquired frequency data at two-second intervals, over a total period of six minutes. In some cases, immediately after the additions of turbidimetric solution inside the probe, much higher values of frequency were detected (Figure 9).

Figure 9 – Raw frequency data captured by the TCS230 sensor, during the entirety of an experiment, for the red spectrum considering the emission of white light (Experiment carried out on May 16, 2025).

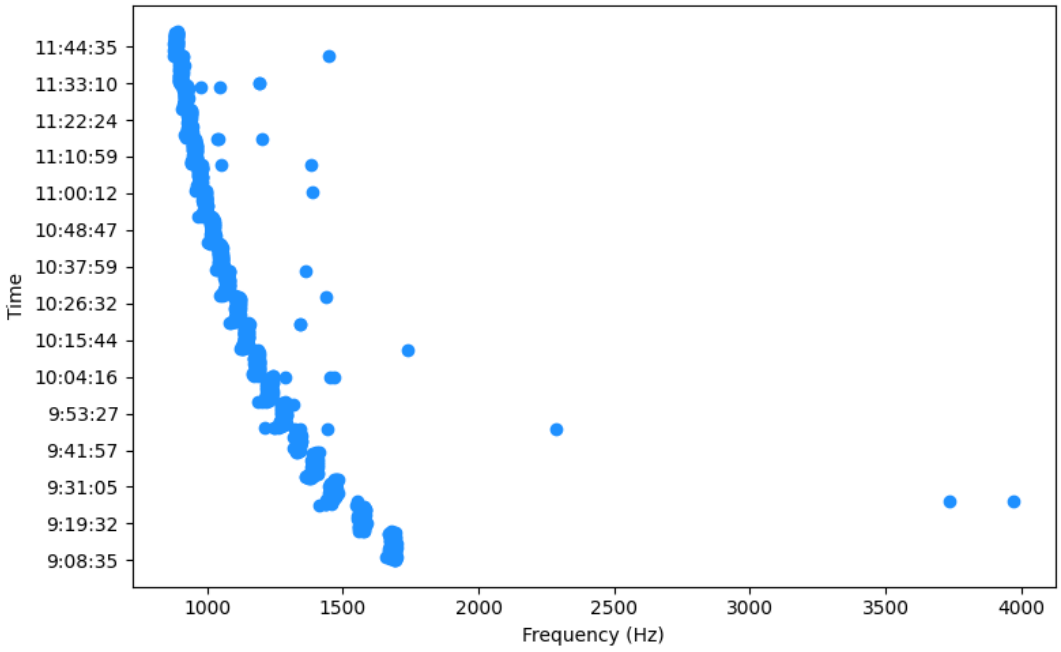


To minimize the influence of these outliers, a stabilization period of three minutes was defined following each addition. A single representative frequency value was adopted for each step, defined as the mean frequency recorded during the subsequent three-minute interval. This procedure also facilitated future analysis, allowing each step to be represented by a single value for volume, turbidity, and frequency.

Along the experiments, the frequency output consistently exhibited an exponential decrease with increasing turbidity (Figure 10). The nephelometric principle, on which the system is based, involves measuring light scattered at a specific angle (in this study, 90°) relative to the incident beam. At higher concentrations of suspended solids—and thus greater turbidity—more particles scatter or absorb the emitted light, reducing the frequency signal detected by the photodetector. The observed results confirmed this behavior, indicating that the probe functions according to nephelometric principles.

Also, for the different combinations of emission colors and intensities measured by the TCS230 sensor, different sensitivities and detection ranges were noted, demonstrating that light scattering depends, among other factors, on the wavelength.

Figure 10 – Relation between the concentration of turbidimetric solution added inside the prototype and the turbidity measured by the commercial turbidimeter with the frequency captured by the sensor for the red spectrum considering the emission of a-b) white, c-d) green and e-f) red light. The horizontal bars indicate the standard deviation of the measurements for each round of the experiment (Experiment carried out on May 16, 2025)

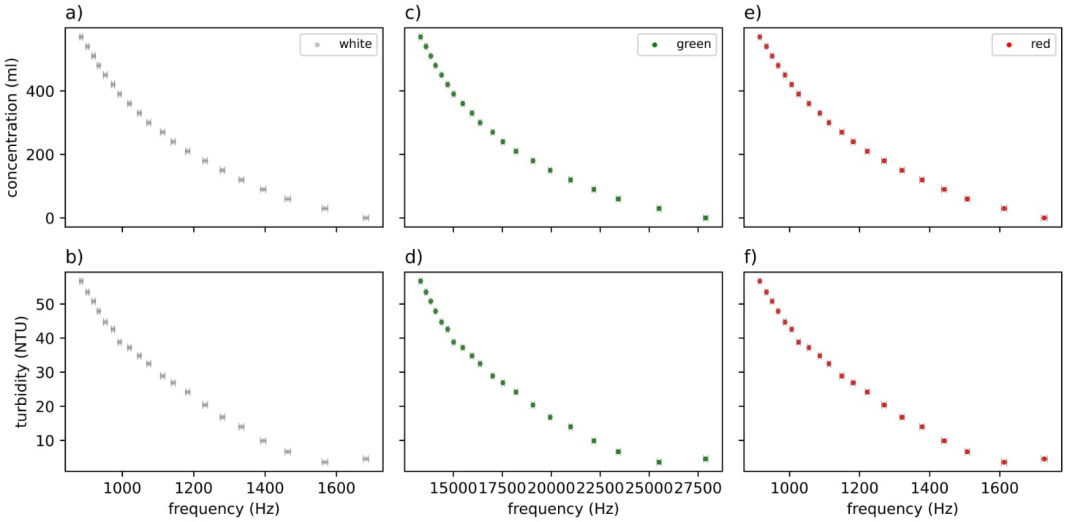


## 4.2 Prototype calibration

### 4.2.1 Calibration curves

To describe the prototype's behavior, two exponential regressions (Equation 4.1) were adopted: one applied to the turbidity range 0–80 NTU and another for 80–200 NTU (Figure 11). Other regressions and models types, including the Four-Parameter Logistic (4PL) model, were initially evaluated and yielded similar performance; however, the exponential form was selected due to its lower number of parameters and simpler calibration procedures.

$$T(f) = ae^{bf} \tag{4.1}$$

where $T$ is the predicted turbidity given in Nephelometric Turbidity Unit ($NTU$), $f$ is the output frequency from the TCS230 sensor, given in Hertz ($Hz$), and $a$ and $b$ are respectively, the y-intercept (the value of the function when $f$ is zero) and the decay rate.

Considering the nine possible emitter–receptor combinations, the coefficient of determination ($R^2$) ranged from 0.975 to 0.989 for the interval of $0 - 80$ NTU, with a mean value of $0.985 \pm 0.005$, while for the 80–200 NTU range, $R^2$ fluctuated from 0.987 to 0.993, with an average value of $0.990 \pm 0.003$. Considering the total evaluated range ($0 - 200$ NTU), $R^2$ varied from 0.983 to 0.992, with a mean value of $0.988 \pm 0.003$. The lowest $R^2$ values were consistently associated with green emission and red reception, whereas the best performance was obtained for red emission and clear reception.

The resulting parameters for all combinations are presented in Table 5.

The red-green combination was excluded from the analysis because the sensor output frequency likely exceeded the numerical limit of the register, presenting negative values and resulting in invalid readings and unreliable calibration.

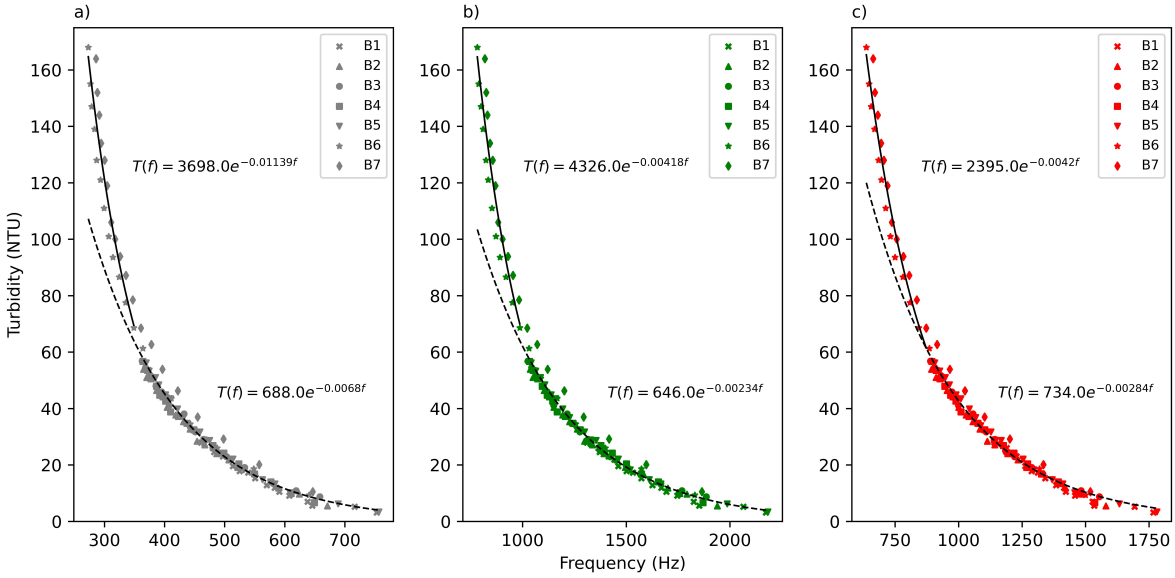


Figure 11 – Relationship between the output frequency signal captured by the sensor for the clear spectrum and the turbidity measured by the commercial turbidimeter, for the emission of: a) white, b) green, and c) red light. For each combination, the exponential regressions for the ranges 0–80 NTU (dashed black lines) and 80–200 NTU (continuous black lines) are shown

Table 5 – Exponential parameters and coefficient of determination ($R^2$) for each wavelength range captured and emitted for the different turbidity ranges.

| Wavelengths | | **Curve 1 (0-80 NTU)** | | | **Curve 2 (80-200 NTU)** | | | **Total (0-200 NTU)** |
|---|---|---|---|---|---|---|---|---|
| Emitted | Captured | $a$ | $b$ | $R^2$ | $a$ | $b$ | $R^2$ | $R^2$ |
| White | Red | 934 | -0.00313 | 0.988 | 2967 | -0.00447 | 0.992 | 0.991 |
| | Green | 594 | -0.00185 | 0.984 | 4315 | -0.00342 | 0.988 | 0.987 |
| | Clear | 688 | -0.0068 | 0.985 | 3698 | -0.01139 | 0.988 | 0.988 |
| Green | Red | 768 | -0.00019 | 0.975 | 3491 | -0.00031 | 0.987 | 0.983 |
| | Green | 608 | -0.0014 | 0.985 | 3967 | -0.00251 | 0.988 | 0.987 |
| | Clear | 646 | -0.00234 | 0.986 | 4326 | -0.00418 | 0.987 | 0.987 |
| Red | Red | 964 | -0.00306 | 0.988 | 2875 | -0.00428 | 0.993 | 0.991 |
| | Green | - | - | - | - | - | - | - |
| | Clear | 734 | -0.00284 | 0.989 | 2395 | -0.0042 | 0.993 | 0.992 |

### 4.2.2 Prototype validation

Validation was performed by comparing the turbidity measured by the DLT-WV digital sensor with the turbidity predicted by the calibrated probe, using the exponential regressions (Figure 12).

Considering the absolute error calculated for the validation data, the lower turbidity range presented better results, with values tipically bellow the 5% threshold up to almost 50 NTU, while for the higher turbidity values, some combinations presented absolute errors above the 10% threshold.

For the eight viable combinations, the $0 - 80$ NTU interval presented minimum and maximum $RMSE$ (Table 6) values of 2.1710 and 4.4976 NTU, with an average of 2.7983 $\pm$ 0.7507, while for the higher turbidity range, the mean $RMSE$ was 12.0369 $\pm$ 0.7611, with values fluctuating from 10.8876 to 13.0369 NTU. Considering the entire turbidity spectrum explored, the $RMSE$ varied between 6.7121 and 8.3769 NTU, with an average of 7.4390 $\pm$ 0.5253 NTU.

For the lower range, the $MAE$ (Table 7) and $MAPE$ (Table 8) obtained values went from 1.6325 to 3.6356 NTU and 6.0195 to 13.1215 %, with mean values of 2.1733 $\pm$ 0.6349NTU and 9.0513 $\pm$ 2.6615%, respectively. For the $80 - 200$ NTU interval, they went from 8.8205 to 11.0948 NTU and 6.8174

Figure 12 – Comparison between the turbidity measured by the commercial turbidimeter (y-axis) and the turbidity predicted by the calibration curves (x-axis) obtained using the exponential models for the clear receptor (without the use of filters), and for a) white, b) green, and c) red emissions. The 1:1 black line indicates a perfect match between predicted and measured turbidity values. Colored solid lines represent the absolute error (secondary y-axis) across various turbidity ranges, while the blue and red dashed lines denote error thresholds of 5% (commonly achieved by commercial turbidity meters) and 10% (typical for low-cost turbidity probes), respectively.

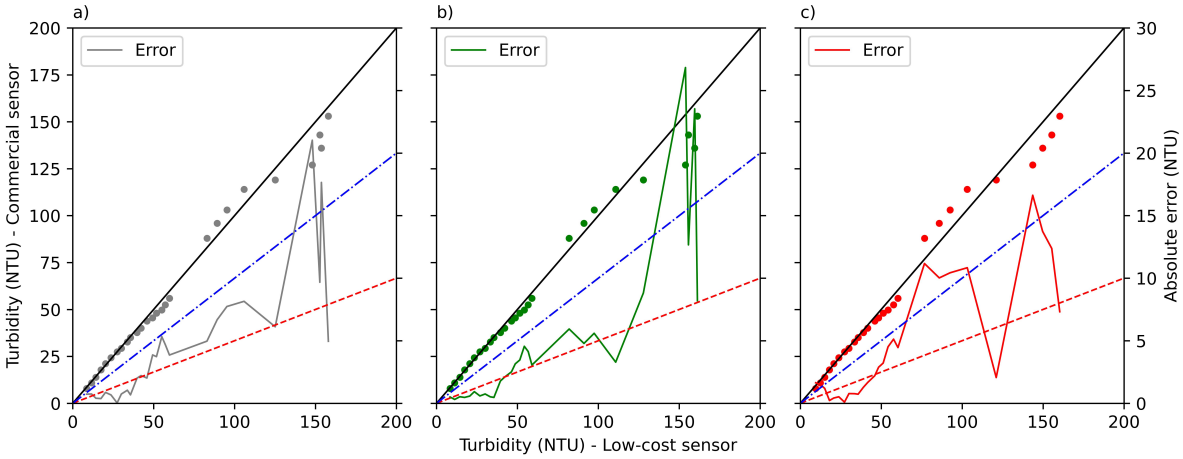


Table 6 – $RMSE$ values for each wavelength captured and emitted, their average value and their respective standard deviation ($\sigma$) for all turbidity ranges.

| Wavelengths | | $RMSE$ ($NTU$) | | | | | | | | |
|---|---|---|---|---|---|---|---|---|---|---|
| Emitted | Captured | Curve 1 ($0-80$ NTU) | | | Curve 2 ($80-200$ NTU) | | | Total ($0-200$ NTU) | | |
| | | Values | Mean value | Standard deviation ($\sigma$) | Values | Mean value | Standard deviation ($\sigma$) | Values | Mean value | Standard deviation ($\sigma$) |
| | Red | 2.9833 | | | 11.7163 | | | 7.2915 | | |
| White | Green | 2.4251 | | | 12.2955 | | | 7.4823 | | |
| | Clear | 2.5245 | | | 10.8876 | | | 6.7121 | | |
| | Red | 4.4976 | | | 12.8478 | | | 8.3769 | | |
| Green | Green | 2.1710 | 2.7983 | 0.7507 | 12.4204 | 12.0369 | 0.7611 | 7.5022 | 7.4390 | 0.5253 |
| | Clear | 2.2343 | | | 13.0369 | | | 7.8663 | | |
| | Red | 2.9949 | | | 11.9062 | | | 7.3999 | | |
| Red | Green | - | | | - | | | | | |
| | Clear | 2.5559 | | | 11.1750 | | | 6.8805 | | |

Table 7 – $MAE$ values for each wavelength captured and emitted, their average value and their respective standard deviation ($\sigma$) for all turbidity ranges.

| Wavelengths | | $MAE$ ($NTU$) | | | | | | | | |
|---|---|---|---|---|---|---|---|---|---|---|
| Emitted | Captured | Curve 1 ($0-80$ NTU) | | | Curve 2 ($80-200$ NTU) | | | Total ($0-200$ NTU) | | |
| | | Values | Mean value | Standard deviation ($\sigma$) | Values | Mean value | Standard deviation ($\sigma$) | Values | Mean value | Standard deviation ($\sigma$) |
| | Red | 2.2947 | | | 10.9172 | | | 5.2680 | | |
| White | Green | 1.8554 | | | 9.5361 | | | 4.5039 | | |
| | Clear | 1.9407 | | | 9.5679 | | | 4.5708 | | |
| | Red | 3.6356 | | | 8.8205 | | | 5.4235 | | |
| Green | Green | 1.6325 | 2.1733 | 0.6349 | 9.5029 | 10.0680 | 0.8153 | 4.3464 | 4.8956 | 0.4089 |
| | Clear | 1.7408 | | | 10.5482 | | | 4.7778 | | |
| | Red | 2.2708 | | | 11.0948 | | | 5.3136 | | |
| Red | Green | - | | | - | | | | | |
| | Clear | 2.0159 | | | 10.5564 | | | 4.9609 | | |

to 9.8788%, with averages of 10.0680 ± 0.8153 NTU and 8.5799 ± 1.1133%, respectively. Considering the total interval, the $MAE$ ranged from 4.3464 to 5.4235 NTU, with a mean of 4.8956 ± 0.4089 NTU and the $MAPE$, varied between 6.6079 and 10.9476%, with an average of 8.887 ± 1.8514%.

For each turbidity interval, the overall performance was broadly comparable, with all exhibiting similar $RMSE$, $MAE$ and $MAPE$ values. For the lower range, the best performance was observed for the green-green pair, which presented the lowest values for the three metrics, while the worst results were observed for the red-green reception-emission combination, which in turn, exhibited the highest metrics values. For the higher turbidity values, the red-green and clear-white reception-emission combinations presented the best results, with the first having the best $MAE$ and $MAPE$ values, while the second,

Table 8 – $MAPE$ values for each wavelength captured and emitted, their average value and their respective standard deviation ($\sigma$) for all turbidity ranges.

| Wavelengths | | $MAPE$ (%) | | | | | | | | |
|---|---|---|---|---|---|---|---|---|---|---|
| Emitted | Captured | Curve 1 (0 – 80 NTU) | | | Curve 2 (80 – 200 NTU) | | | Total (0 – 200 NTU) | | |
| | | Values | Mean value | Standard deviation ($\sigma$) | Values | Mean value | Standard deviation ($\sigma$) | Values | Mean value | Standard deviation ($\sigma$) |
| White | Red | 11.2649 | 9.0513 | 2.6615 | 8.8495 | 8.5799 | 1.1133 | 10.7768 | 8.8887 | 1.8514 |
| | Green | 6.5020 | | | 7.8408 | | | 6.9637 | | |
| | Clear | 7.6335 | | | 8.2603 | | | 7.8497 | | |
| Green | Red | 13.1215 | | | 6.8174 | | | 10.9476 | | |
| | Green | 6.0195 | | | 7.7259 | | | 6.6079 | | |
| | Clear | 6.7721 | | | 8.7588 | | | 7.4572 | | |
| Red | Red | 11.1569 | | | 9.8788 | | | 10.7161 | | |
| | Green | - | | | - | | | | | |
| | Clear | 9.9400 | | | 9.5074 | | | 9.7908 | | |

presented the lowest $RMSE$ value for this turbidity range.

Considering the entire analysis scope, the overall best performance was observed for the green-green combination, which presented the best $MAE$ and $MAPE$ and for the clear-red pair, which exhibited the lowest $RMSE$ value. Even though the data obtained for the green reception and red light emission exhibited good results for the $80 - 200$ NTU, it performed the worst for the total interval.

For the analyses, the obtained results for the $0 - 200$ NTU range were closer to those observed in the lower interval, due to the higher quantity of data for it.

## 4.3 Algae detection

### 4.3.1 Algae experiments

For the algae experiments, the relationship between the output frequency and turbidity was confronted with the calibration curves obtained for each emitter–receptor pair (Figure 13).

Figure 13 – Comparison between turbidity measured by the commercial turbidimeter and frequency outputs for a) white, b) green, and c) red emissions, targeting the clear receptor. The black dashed lines indicates the curves obtained during calibration for each combination for the $0 - 80$ NTU range, and the different symbols (cross, triangle, circle, square and inverse triangle) represent the data acquired during different experiments, with distinct algae concentrations.

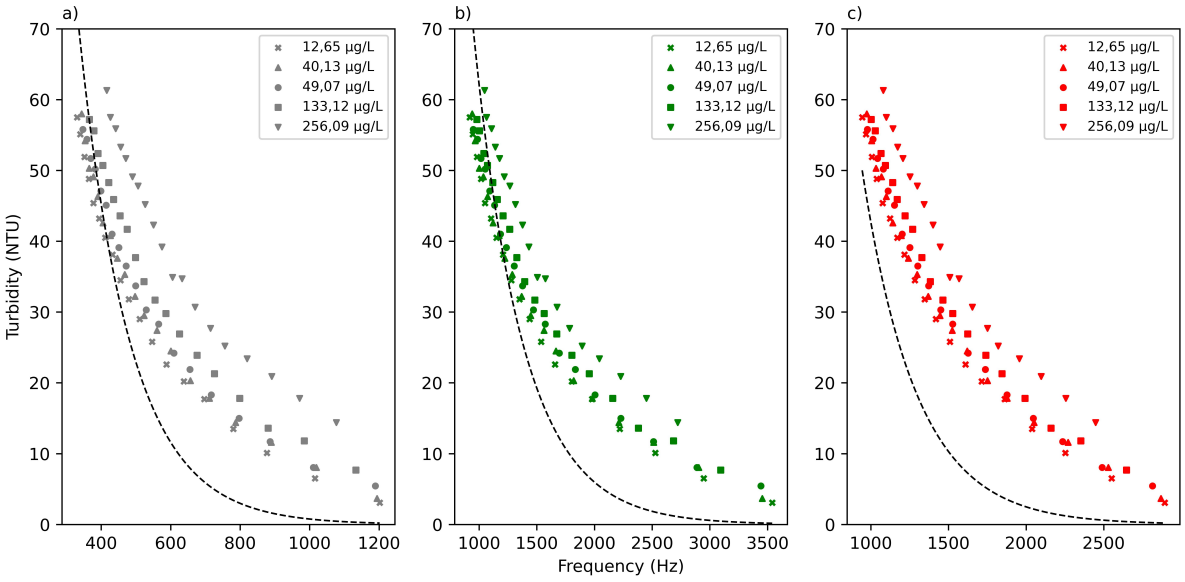

Unlike the calibration experiments, which used only formazin solutions, the algae tests did not produce the expected frequency responses when individual channels (green, red, or clear) were analyzed. It was initially hypothesized that higher algae concentrations would result in greater light absorption (particularly at red wavelengths) and/or increased scattering (especially at green wavelengths), which in turn would decrease the output frequency, associated with the intensification of the green component within the RGB spectrum. However, the probe exhibited the opposite trend: higher concentrations of algae resulted in increased frequency outputs (Figure 13).

This behavior may be attributed to the combined effects of the TCS230 spectral sensitivity and the distinct optical properties of algae relative to formazin. The filters on the TCS230 sensor (red, green, and clear) do not have sharply defined spectral boundaries and exhibit overlapping sensitivity ranges (Figure 14). For instance, although the red channel is most sensitive to wavelengths around 600–750 nm, it still detects portions of the green spectrum near 580–600 nm.

Figure 14 – Spectral responsivity graphic for the TCS230 photodiode, that indicates for what wavelengths, each detecting range (blue, green, red and clear) presents the higher or lower values of relative responsibility.

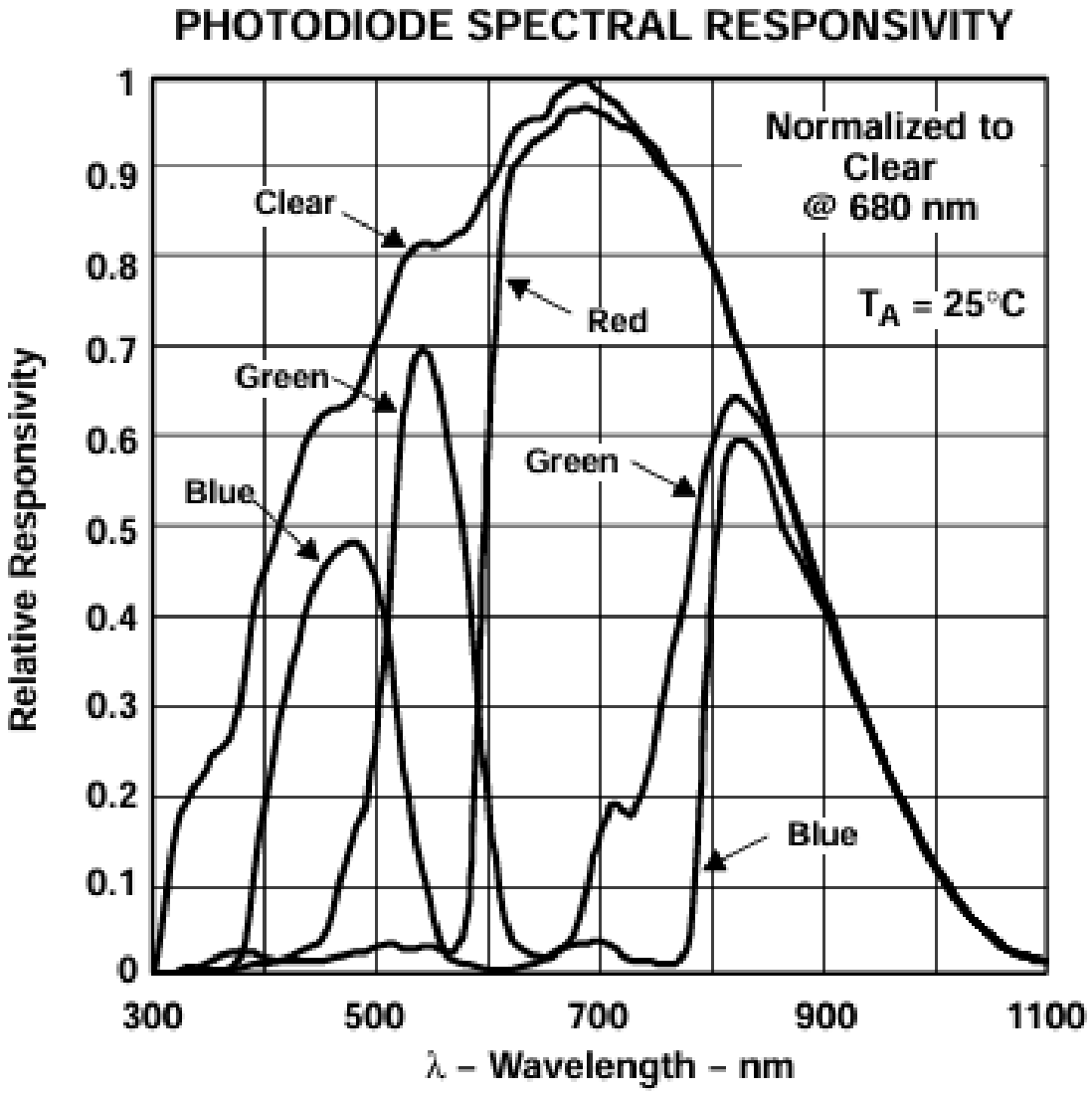

Furthermore, in contrast to formazin, which scatters light uniformly across the visible spectrum, green algae absorb light predominantly in the red and blue ranges while reflecting green light (particularly between 500 and 600 nm), following the typical absorption spectrum of chlorophylls a and b (Figure 15). Due to spectral overlap, reflected green light was possibly detected not only by the green filter but also partially by the clear and red filters, therefore increasing output frequency under higher chlorophyll concentrations.

Figure 15 – Absorption spectrum of chlorophyll A and B. Source: Panawala (2017)

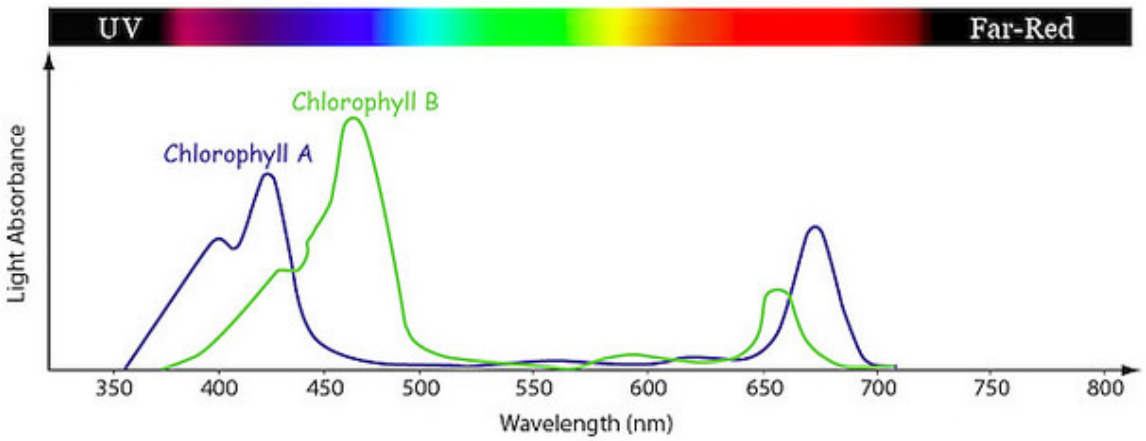


Considering the three emitted colors (white, green and red), for white emission, which includes all visible wavelengths, and for green emission, where green is dominant,the green component is reflected, not being absorbed at any rate, and since all three filters (R, G, and C) are sensitive in this wavelength range (500–600 nm), the overall frequency outputs are higher. Even for red LED emission, due to slight spectral overlap, some green light is still captured, which also leads to increased output frequency at higher algae concentrations.

So, for the purpose of algae detection, instead of utilizing single-frequency outputs separately, the ratios between the output frequencies of the green and clear channels ($f_G/f_C$), as well as the green and red channels ($f_G/f_R$) for the white and green emissions were evaluated. The ratio $f_G/f_C$ under white illumination exhibited the highest consistency and discriminative capability, including at low turbidity, and was therefore, adopted as the primary indicator of chlorophyll concentration.

Samples with higher total chlorophyll concentrations exhibited higher frequency responses across all RGB components (Figure 13). As seen during the calibration and validation phases, the output frequency was shown to be inversely proportional to the intensity of the captured color component. Subsequently, lower $f_G/f_C$ (Figure 16a) ratios were observed under high chlorophyll conditions.

To describe and calibrate the overall chlorophyll response as a function of turbidity and frequency ratio, considering both nonlinear and interactive effects, a double-exponential mixed model was proposed (Equation 4.2):

$$C(f,T) = a_0 + a_1 \ \exp\{(-a_2 \ (f-3.1))\} + a_3 \ \exp\{(-a_4 \ T)\} + a_5 \ \exp\{(-a_6 \ T(f-3.1))\} \qquad (4.2)$$

where $T$ is the turbidity (NTU) calculated using the calibration curves, and $f$ is the non-dimensional green-to-clear frequency ratio, under white-LED illumination. The coefficients $a_0$ - $a_6$ were

Figure 16 – Correlation between the frequencies ratios between green and clear components ($f_G/f_C$) for white emission and the turbidity measured by the digital sensor, for different total chlorophyll concentrations.a) The baseline was obtained using the calibration curves and the overall results acquired during calibration (purple dots), for the experiments using only formazin, and was considered as the 0 $\mu$g/l mark. The colored dashed lines represents the exponential regression curves obtained for each concentration, while the gray scatter points indicates the data from each respective experiment. The experiments A1, A2 , A3, A4 and A5 presented initial total chlorophyll concentrations of 40.13, 12.65, 49.07, 133.12 and 256.09 $\mu$g/l, respectively. b) Calibrated map using the model presented in Equation 4.2.

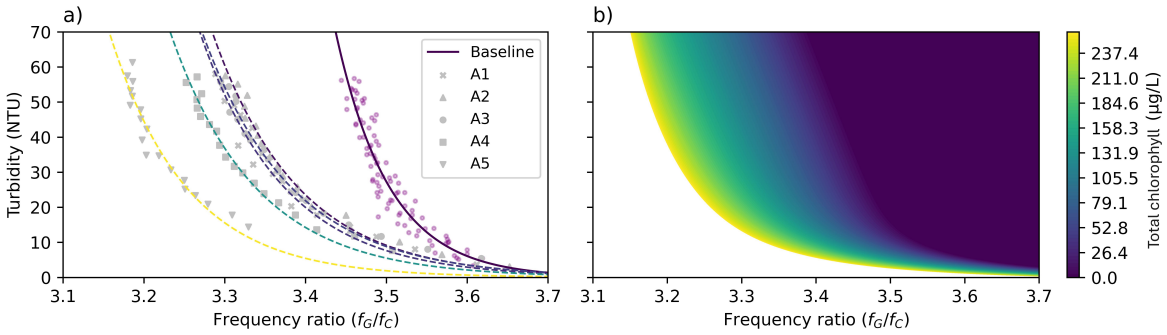


obtained through nonlinear least-squares regression using the Levenberg-Marquardt optimizer algorithm. Negative values of $C(f,T)$ were set to $C(f,T) = 0$.

The use of ratios also made it possible to distinguish between turbidity sources and total chlorophyll concentrations at lower turbidities and with higher confidence intervals, due to the more significant separation between the curves, when in comparison with the observed for the single outputs frequencies (Figure 13).

### 4.3.2 Green dye experiments

For the green dye experiments, the relationship between the output frequencies and turbidity was compared with the calibration curves obtained for each emission-reception combination (Figure 17).

As in the algae tests, higher dye concentrations resulted in increased sensor frequencies, reflecting the strong green spectral component of the dye and the overlapping sensitivity of the TCS230 filters During these tests, samples of the green dye solutions were measured for total chlorophyll using the digital fluorometer, nonetheless, due to the negligible chlorophyll concentration in its composition, the obtained results were not representative, nor consistent, and were therefore, disregarded for analysis.

## 4.4 Continuous monitoring tests

During the continuous monitoring tests, changes in the probe's response and output frequencies were detected and multiple diagnostic evaluations were conducted in order to determine the origin of these discrepancies, including: tests in different experimental environments, tests with other microcontrollers of the same model and other electronic components, and visual inspections of all the probe's components. Nonetheless, the causes could not be determined during the scope of this project, and to avert unreliable and inconsistent measurements during the continuous monitoring tests, a new set of experiments were conducted to adjust the exponential regressions. The obtained curves yielded equivalent and consistent results and statistical metrics in comparison with the previous calibration and validation results.

Figure 17 – Comparison between turbidity measured by the commercial turbidimeter and frequency outputs for a) white, b) green, and c) red emissions, targeting the clear receptor. The black dashed lines indicates the curves obtained during calibration for each combination for the $0 - 80$ NTU range, and the different symbols (cross, triangle, circle and square) represent the data acquired during different experiments, with distinct green dye concentrations.

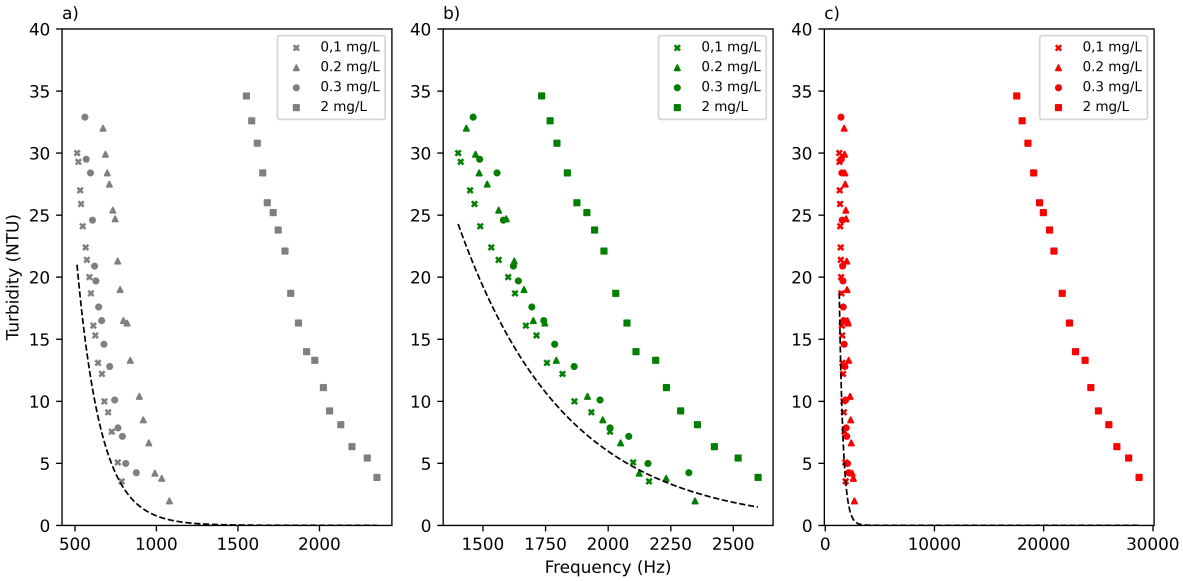


In the first experiment (Figure 18), turbidity remained near 0 NTU during the initial steady-state period. Approximately ten minutes after the turbidimetric solution began to be injected into the tank, turbidity inside the tank peaked at 33.35 NTU, and subsequently, decreased to approximately 9.815 NTU following the injection of clean water into the system. In comparison, for the calculated turbidity, the highest values (considering the mean value obtained by all emission-reception pairs), were close to 25.5 NTU, and were detected nearly 25 minutes after the injection had began, while at end, the calculated turbidity, was 19.1282 NTU.

For this test, due to the significant higher flow (around 47 l/h or 0.000013 $m^3/s$), the turbidimetric solution was rapidly depleted in a few minutes, causing a steep turbidity increase that the probe could not fully track, resulting in a tangible response lag.

For the second test (Figure 19), as the average injection flow was reduced, a slower turbidity increase rate was observed, with a turbidity peak of 52.95 NTU being detected 50 min into the experiment. With the addition of clean water, the turbidity gradually decreased, reaching values close to 19.1 NTU at the end of the test.

For the calculated turbidity, maximum values of about 67.1274 NTU were identified nearly 60 minutes after the experiment began, while at the end, the calculated turbidity was 43.8815 NTU. Even though in this test, with a lower flow, the sensor was capable of quite accurately predict the turbidity increase, for its second phase, with the addition of clean water, it still overestimated turbidity, presenting higher values than those observed and measured using the digital sensor.

In the third experiment (Figure 20), a turbidity peak of 63.65 NTU was observed nearly 70 min into the test. The system kept circulating clean water for approximately 25 min before the injection of the formazin turbidimetric solution at 13:26:30, while the algae was added in the inlet bucket roughly 24 min after this, at 13:50:00. With the injection of clean water, the turbidity gradually decreased, reaching values up to 21.8 NTU

Figure 18 – Turbidity variation throughout the duration of the first continuous experiment for clear reception and for emission of white, green and red, from up to bottom, respectively. The dots represent the average turbidity values measured from the probe's inlet and outlet at each step, with the vertical lines being its standard deviation. The solid lines represent the turbidity as calculated using the calibration curves.

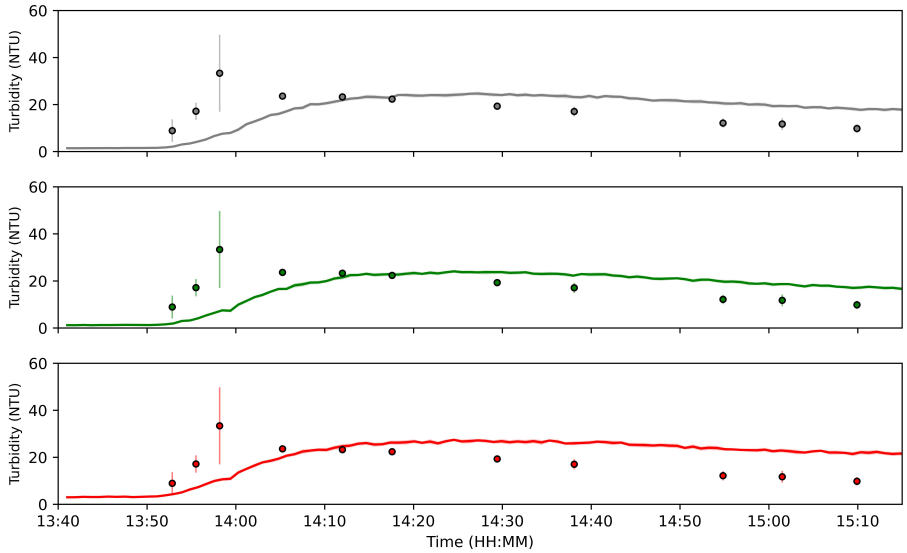


Table 9 – $RMSE$, $MAE$ and $MAPE$ mean values obtained for each continuous experiment, and their respective standard deviation ($\sigma$).

| Experiments | Metrics | | | | | |
|---|---|---|---|---|---|---|
| | RMSE($NTU$) | | MAE ($NTU$) | | MAPE (%) | |
| | Mean value | Standard deviation ($\sigma$) | Mean value | Standard deviation ($\sigma$) | Mean value | Standard deviation ($\sigma$) |
| Experiment 1 | 10.3656 | 0.1407 | 8.3129 | 0.5618 | 51.2176 | 5.1708 |
| Experiment 2 | 18.4473 | 5.6937 | 16.1209 | 5.9277 | 55.0013 | 18.9910 |
| Experiment 3 | 11.9911 | 3.9629 | 9.6204 | 3.2303 | 30.6457 | 8.8190 |

For the calculated turbidity, the addition of algae did not interfere on the results or provoked any displacements on the obtained curve. The maximum calculated values, revolved around 58.42 NTU and were detected about 65 minutes after the initial injection of the formazin-only solution, occurring roughly 10 minutes after the measured peak.

At the experiment's end, the average calculated turbidity was close to 45.56 NTU, exhibiting similar behavior to the previous tests, where the probe exhibited faster responsiveness during turbidity increases and slower adaptation during dilution phases, leading to response lags. This may indicate a tendency in the current probe's design to accumulate and retain sediments inside the monitoring area.

For each experiment, the turbidity values measured by the commercial sensor were compared with those calculated by the probe over the same time periods, and the same statistical metrics employed during calibration and validation (Table 9) were adopted. The lowest $RMSE$ and $MAE$ were obtained for the first experiment, likely due to the lower turbidity achieved and the overall smaller difference between the calculated and observed values, especially for the second phase of the test. Alternatively, the best $MAPE$ performance was observed for the third experiment, possibly due to the higher magnitude of the measured turbidity.

The probe was configured to record, every 15 minutes, the maximum chlorophyll concentration

Figure 19 – Turbidity variation throughout the duration of the second continuous experiment for clear reception and for emission of white, green and red, from up to bottom, respectively. The dots represent the average turbidity values measured from the probe's inlet and outlet at each step, with the vertical lines being its standard deviation. The solid lines represent the turbidity as calculated using the calibration curves.

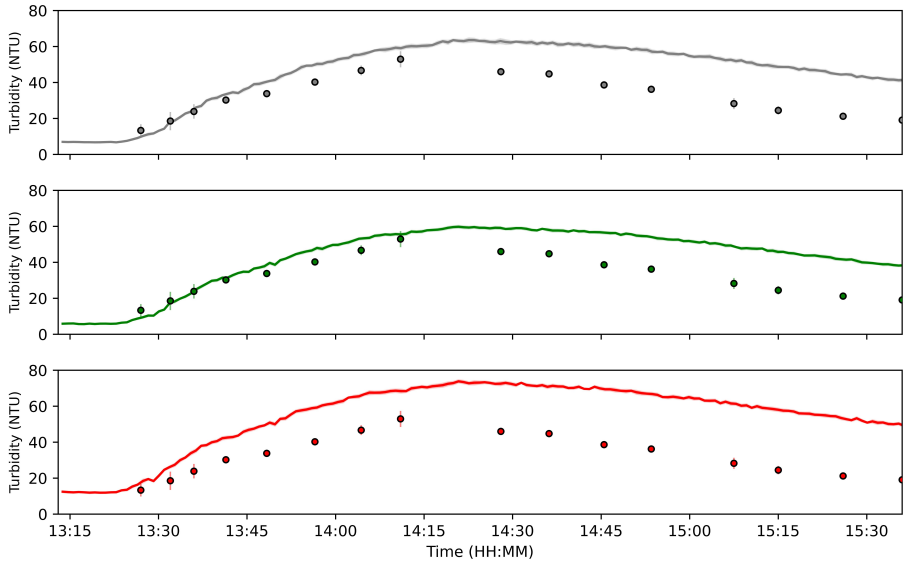


detected during the sampling interval.The estimated total chlorophyll concentration values ($C(f,T)$) were negative throughout the majority of the experiment, only presenting a response near the total chlorophyll observed peak (Figure 21). Measured chlorophyll reached a maximum value roughly 23 minutes after algal initial addition, with concentrations up to 90.97 $\mu$g/l. In comparison, the highest calculated concentration was approximately 50 $\mu$g/l and was detected nearly sixteen and a half minutes after the observed maximum. Although not quantitatively precise, the probe successfully detected substantial total chlorophyll increases for concentrations close to, or above 50 $\mu$g/l, demonstrating its ability to identify algal bloom-like events.

Figure 20 – Turbidity variation throughout the duration of the third continuous experiment for clear reception and for emission of white, green and red, from up to bottom, respectively. The dots represent the average turbidity values measured from the probe's inlet and outlet at each step, with the vertical lines being its standard deviation. The solid lines represent the turbidity as calculated using the calibration curves.

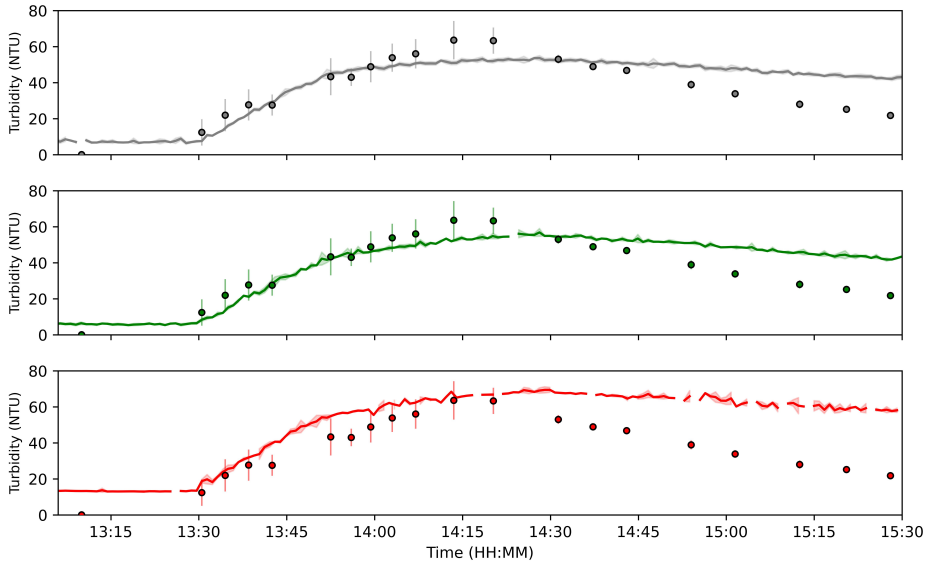


Figure 21 – Total chlorophyll and turbidity variation throughout the test. a) The solid line indicates the turbidity (NTU) obtained using the calibrated curves obtained for the the white–clear emitter–receptor pair. The dots represent the mean turbidity measured by the digital turbidity sensor, and the vertical bars denote the standard deviation from measurements taken at the probe's inlet and oulet. b) The green dots indicate the chlorophyll concentrations measured by the digital fluorometer, while the vertical bars represents the maximum chlorophyll concentration ($C(f,T)$) detected by using the calibrated curve (Eq. 4.2), for the $f_G/f_C$ ratio under white-LED illumination and for the turbidity calculated using the calibration curves for the white-clear pair. The vertical black, green and red dashed lines marks the initial release of the turbidimetric solution (with only formazin), the initial release of the turbidimetric solution containing algae and the injection of clean water into the tank, respectively.

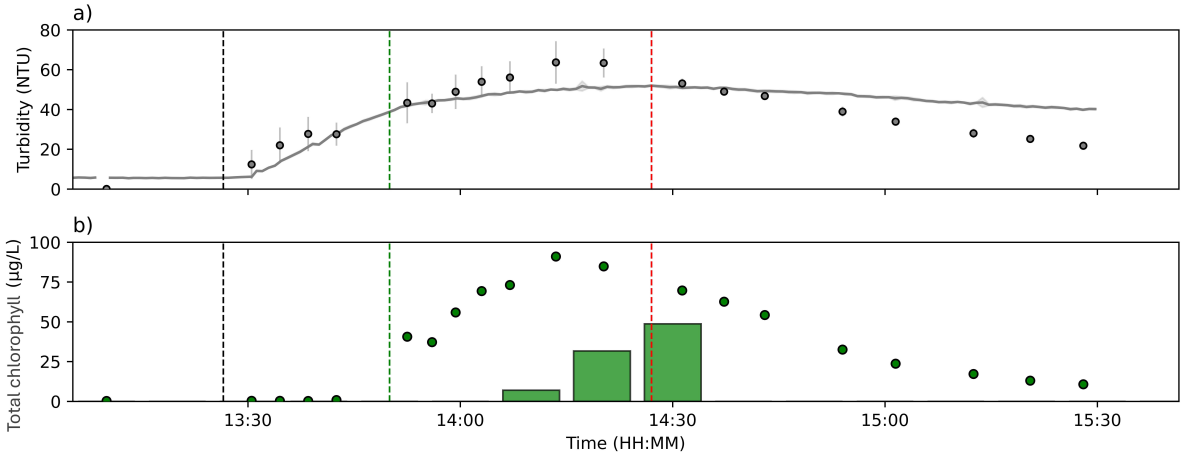

# 5 Discussion

To address the proposed research question, several experimental stages were carried out using the probe, including calibration, validation, algae identification, and continuous monitoring tests. This chapter discusses the experimental findings obtained during each of these steps, examines the primary limitations identified throughout the study, evaluate the feasibility of the proposed approach for continuous monitoring applications, and compares the obtained results with those reported in previous studies on low-cost turbidimeter development.

Table 10 presents an overall comparison between different low-cost sensors proposed in the literature and the one discussed in this study.

## 5.1 Calibration and validation

Previous studies have proposed a wide range of regression models to describe the behavior of different low-cost turbidimeters. The prototype presented in this study yielded consistent calibration results, with coefficients of determination ($R^2$) of 0.985 ± 0.005, 0.990 ± 0.003 and 0.988 ± 0.003 for the $0 - 80$ NTU, $80 - 200$ NTU and $0 - 200$ NTU ranges, respectively. In comparison, Kelley et al. (2014) reported values of $R^2 > 0.9990$ for turbidity above 0.5 NTU, Parra et al. (2018) achieved $R^2$ ranging from 0.984 to 0.999 for a turbidity interval of $0 - 200$ NTU, while Droujko and Molnar (2021) worked with an analysis range of approximately $0 - 4000$ NTU , obtaining $R^2 > 0.98$ for processed data.

For validation, considering the absolute errors between the observed and calculated turbidity values, a better performance was obtained for the calibration curves encompassing the lower range. Even though the higher interval, worst absolute errors, it also comparatively, presented the lowest relative errors, largely due to the higher magnitude of turbidity values in this interval. For turbidity standards of 100 NTU, Kelley et al. (2014) obtained $RMSE$ values of 9.54 NTU, which is comparable to the average $RMSE$ of 12.0369 ± 0.7611 NTU obtained in this study. On the other hand, Droujko and Molnar (2021) achieved relative errors below ±5% for processed data, while Parra et al. (2018) reported $MAE$ values up to 0.65 NTU, with both presenting slightly better results in comparison with this sensor.

Despite these minor differences, the performance of the proposed sensor and calibration models was strong and aligned with the range of accuracies typically reported for low-cost turbidity sensors. These results confirm that the prototype can reliably estimate turbidity within the defined measurement range for non-continuous monitoring.

## 5.2 Continuous monitoring

Throughout the continuous monitoring experiments, the probe successfully detected both increases and decreases in turbidity within the tank, although a response lag was consistently observed, particularly under lower flow rates. Statistically, considering the average error values obtained for the lower turbidity range during calibration and validation, for continuous monitoring these errors were three to seven times higher, indicating a considerable decline in accuracy and quantification performance under dynamic conditions.

Within the scope and duration of this project, it was not possible to conduct enough tests to determine with exactitude, the causes of the observed response lag. Nonetheless, the primary hypothesis attributes this behavior to the retention of suspended solids within the probe due to its current design, particularly the presence of the maze-like pattern.

For continuous monitoring, Gillett and Marchiori (2019) reported median residual and standard deviation for the inlet and outlet utilized sensors of -0.4507, 1.9063 NTU and 1.3997, 6.5511 NTU, respectively. In the mentioned study, it was also noted better performance under controlled calibration conditions.

## 5.3 Algae identification

During the initial algae tests, it was noticed that single-frequency outputs did not adequately describe or present the expected results for different chlorophyll concentrations. As a result, the ratio between green and clear channel frequencies ($f_G/f_C$), particularly under white LED illumination, was adopted. Calibration comprised total chlorophyll concentrations between 0 (baseline) and 256.09 $\mu$g/l. By using the ratio, it was possible to differentiate between turbidity sources and chlorophyll concentrations for turbidity values near or above 5 NTU. These results slightly surpass those reported by Parra et al. (2018), who achieved turbidity-source differentiation above 12 NTU.

Green dye tests were conducted to explore whether food coloring could replace algae in calibration procedures. However, comparisons between dye and algae responses revealed substantial differences in the sensor's behavior, demonstrating that green dye cannot replicate the optical properties of algae for calibration purposes. Even though for the sensor composition and design, green dye could not replace algae during calibration, these experiments highlighted that the coloration of a solution may influence the probe's operation and results.

Algae identification was further evaluated during continuous monitoring. Although the initially proposed model for calculating concentrations did not accurately quantify or fully track the chlorophyll variation throughout the test, the probe was capable of detecting a chlorophyll peak derived from the algae injection into the tank, despite the continued presence of response lag. Importantly, the addition of algae did not introduce noticeable noise into the turbidity measurements, indicating that algae presence does not compromise turbidity estimation under the tested conditions.

## 5.4 Research and sensor limitations

In this section, a series of limitations that were found throughout the multiple stages of this study or issues that may pose constraints in future applications are described, and possible solutions are proposed.

The digital fluorometer used in this study measured total chlorophyll, which guided all subsequent analyses. However, nationwide, some of the most relevant regulations focused on water quality and water bodies classification, like the Resolution No. 357 of March 17, 2005, issued by CONAMA and the Consolidation Ordinance No. 5/17 of the Brazilian Ministry of Health, address exclusively the concentration of chlorophyll-a, which is only one of total chlorophyll components. Additionally, agencies such as CETESB, also adopt chlorophyll-a in the calculation of indexes as the Trophic State Index (TSI). Even though total chlorophyll concentrations may be associated with algal incidence in aquatic environments, as it cannot be directly confronted with national regulations, nor is it widely adopted in indexes calcula-

tions, this may eventually narrow the scope of application for the sensor. Since no universal and constant ratio between total chlorophyll and chlorophyll-a for freshwater ecosystems exists, a viable path would be to turn once again to bibliographical research, targeting studies and articles that might evaluate this relation, presenting empirical solutions, that could satisfactorily be applicable to the intended monitoring environment.

The calibration range adopted in this study (0–200 NTU) is consistent with similar works (PARRA et al., 2018; GILLETT; MARCHIORI, 2019). While this range is suitable for monitoring freshwater reservoirs used for drinking-water supply, where relatively high turbidity values are uncommon. For applications in rivers and especially lakes, where higher turbidity values may be expected due to phenomena like algal-blooms, broader turbidity ranges may be necessary. For situations like these, the exponential regression model should be re-evaluated, and additional exponential calibration curves may be required to accurately represent the sensor response across higher turbidity values. Kelley et al. (2014), for example, used a similar light-to-frequency detector in a nephelometric setup and successfully measured turbidity up to 1100 NTU for non-continuous monitoring system, suggesting that expanding the calibration range may be feasible.

The main limitations identified during continuous monitoring were the response lag and the limited accuracy of total chlorophyll estimation. The lag was mainly attributed to the retention of suspended solids inside the probe due to its current design, which may require the future installation of an internal wiper to prevent material accumulation inside the sampling area. Furthermore, to eliminate the possible maze-like pattern contribution to this retention, this structure may be removed or redesigned from the probe's current layout, by applying a similar approach, as presented by Droujko and Molnar (2021), where the measurements were performed with the emitter turned on and off, and the difference between both sets was used to reduce solar-radiation effects. For chlorophyll estimation, further analyses should explore alternative parameter sets for the proposed model (Equation 4.2), as well as different modeling approaches, algorithms, or interpolation techniques such as those described by Rocher et al. (2021).

Finally, due to the project timeline, it was not possible to conduct in situ monitoring campaigns to validate and evaluate the sensor response under real environmental conditions for turbidity quantification and algae detection. During the continuous experiments conducted in a controlled environment, it became clear that parameters like the flow, directly influence the probe's operation. In this sense, in situ tests would likely prove to be essential sources of information about the sensor's operation, as they would expose the probe to variable hydrodynamic, optical, and meteorological conditions that could not be fully replicated in a laboratory, including, but not limited to: precipitation, sunlight, sediment heterogeneity, and particle size variability.

Table 10 – Comparison between low cost sensors proposed in different articles and the one described in this study.

| **Category** | **This study** | **Kelley et al. (2014)** | **Parra et al. (2018)** | **Gillett and Marchiori (2019)** | **Rocher et al. (2021)** | **Droujko and Molnar (2021)** |
|---|---|---|---|---|---|---|
| Analysis parameters | Frequency ($Hz$) → Turbidity ($NTU$) | Frequency ($Hz$) → Turbidity ($NTU$) | Resistance variation (Ohms) → Turbidity ($NTU$) | Frequency ($Hz$) → Turbidity ($NTU$) | Resistance variation (Ohms) → Voltage ($V$) → Algae concentration ($mg/L$) | Frequency ($Hz$) → Suspended sediment concentration SSC ($g/L$) |
| Analysis range | 0–200 NTU | 0–1100 NTU | 0–200 NTU | 0.02–100 NTU | 15–4000 mg/l | 0–16 g/l SSC (approximately 0–4000 NTU) |
| Emission | 1 RGB LED (programmed to emit three different light ranges: white, green and red) | 1 infrared LED | 1 infrared LED and 3 visible light LEDs (red, yellow and green) | 1 visible light LED (white) | 1 infrared LED and 5 visible light LEDs (blue, green, yellow, orange and red) | 1 infrared LED |
| Detection | 1 light-to-frequency converter | 1 light-to-frequency converter | 1 photodiode (IR) and 1 LDR (visible light) | 1 ambient light sensor | 1 photodiode (IR) and 5 LDRs (visible light) | 2 light-to-frequency converters |
| Angle between LEDs and sensors | 90° | 90° | 180° | 90° | 180° | 45°, 90° and/or 135° |
| Application | Continuous water quality monitoring and algae detection | Drinking water monitoring in low-income communities or remote areas | Water quality monitoring in aquaculture farms, particularly in saline or coastal water systems | Continuous water quality monitoring | Algae concentration monitoring in irrigation reservoirs | SSC monitoring on alpine river networks |

| **Category** | **This study** | **Kelley et al. (2014)** | **Parra et al. (2018)** | **Gillett and Marchiori (2019)** | **Rocher et al. (2021)** | **Droujko and Molnar (2021)** |
|---|---|---|---|---|---|---|
| Solutions used for calibration or validation | 2 types (calibration and continuous monitoring): Formazin standard (4000 NTU) diluted in water and green algae | 1 type (calibration): Hydrophilic oil diluted in distilled water and 1 type (validation): non-formazin turbidity standards | 3 types (calibration): River sediments (composed mainly of silt, clay, and sand) and two algae species (Isochrysis galbana and Tetraselmis chui) | 1 type (calibration): Formazin standard (4000 NTU) diluted in deionized water and 1 type (continuous monitoring experiment): coffee powder | 2 types (calibration): Sediments and algae (Chlorella vulgaris) | 2 types (calibration): Sediments (feldspar and sediments collected from the Fieschertal channel) |
| Adopted mathematical models | 2 exponential regressions for distinct ranges ($0 - 80$ NTU and $80 - 200$ NTU) | 4 linear regressions for distinct ranges | Exponential regression | Ordinary least squares linear regression | 7 Multiple regression models and neural network | Fourth order multiple linear regression |

| **Category** | **This study** | **Kelley et al. (2014)** | **Parra et al. (2018)** | **Gillett and Marchiori (2019)** | **Rocher et al. (2021)** | **Droujko and Molnar (2021)** |
|---|---|---|---|---|---|---|
| Precision/ Accuracy | For calibration: $R^2$=0.985 ± 0.005 (0–80 NTU) and $R^2$=0.990 ± 0.003 (80–200 NTU). For validation: $RMSE$ = 2.7983 ± 0.7507 NTU, $MAE$ = 2.1733 ± 0.6349 NTU and $MAPE$ = 9.0513 ± 2.6615 % for the 0–80 NTU interval, and $RMSE$ = 12.0369 ± 0.7611 NTU, $MAE$ = 10.0680 ± 0.8153 NTU and $MAPE$ = 8.5799 ± 1.1133 % for the 80–200 NTU interval | $R^2 > 0.9990$ (for turbidity > 0.5 NTU) and $R^2$ = 0.9977 ( for turbidity < 0.5 NTU), 192 out of 200 prototype measurements (96%) fall within 3% or 0.3 NTU of the average measurement obtained by the commercial turbidimeter and RMSE values of: 0.02, 0.08, 0.33, 9.54, and 31.5 NTU for non-formazin turbidity standards of: 0.02, 1, 10, 100, and 1000 NTU, respectively. | for calibration: $R^2$ values of 0.994 (infrared emission) and 0.999 (red emission). And for validation: MAE up to 0.65 NTU and relative errors of 3% (red emission) | For calibration: Able to reliably estimate turbidity within 1 NTU, although some noise was present. And for the continuous monitoring experiment: median residual and standard deviation for the inlet and outlet sensors were -0.4507, 1.9063 NTU and 1.3997, 6.5511 NTU, respectively. | Average error between predicted and observed algae concentration was 36.52 mg/l with a relative error of 12.56 % | Relative errors < ś10% for raw measurements and < ±5% for processed values and $R^2 > 0.98$ |
| Estimated cost | US$ 50 | US$ 25–35 | €8.30 (without microcontroller and casing) | US$ 64 | Not mentioned | 61.37 CHF |

| **Category** | **This study** | **Kelley et al. (2014)** | **Parra et al. (2018)** | **Gillett and Marchiori (2019)** | **Rocher et al. (2021)** | **Droujko and Molnar (2021)** |
|---|---|---|---|---|---|---|
| Telemetry | Future work: WiFi or LoRa communication | WiFi (GPRS) and cellular network (GSM) | Future work: Creation of a a wireless sensor network (WSN) | WiFi communication | Future work: WiFi and LoRa communication | Not implemented |
| Wiper | Future work | Not mentioned | Not mentioned | Not mentioned | Not mentioned | Future work |
| Differentiation between turbidity sources | Able to distinguish between sources for turbidity levels above 5 NTU (During calibration) | Not mentioned | Able to distinguish between the three sources for turbidity levels above 12 NTU | Not mentioned | Neural network and multiple regression models were used to estimate the concentration of alga | Not mentioned |

# 6 Conclusion

This study presented the calibration, validation, and evaluation of a low-cost optical probe designed for turbidity monitoring and qualitative algae detection. Built using LED-based illumination and a TCS230 light-to-frequency sensor arranged in a nephelometric configuration, the prototype demonstrated consistent behavior under controlled conditions. The calibration results showed strong exponential relationships between the sensor output frequency and turbidity measured, with coefficients of determination between 0.985 and 0.990 for the tested turbidity ranges of $0-80$ NTU and $80-200$ NTU, respectively. Validation tests confirmed that the prototype achieves accuracy levels comparable to those of other low-cost turbidimeters, particularly within the $0-80$ NTU interval.

Algae experiments revealed that the optical response of the sensor differs for different turbidity sources. While formazin caused an expected decrease in output frequency, suspensions of green algae produced an increase, attributable to chlorophyll reflectance and the broad spectral bands of the TCS230 filters. By adopting a spectral ratio approach using the green-to-clear channel frequency, it was possible to distinguish between turbidity sources, and total chlorophyll concentrations.

Continuous monitoring tests showed that the prototype responds to turbidity variations, though with a measurable lag especially for higher flows during dilution phases. This behavior was attributed particularly to the retention of suspended solids inside the probe's measuring chamber, due to its current design . The sensor's performance under dynamic conditions was weaker than during calibration, highlighting the need for design refinements to improve flow-through dynamics and reduce residence-time effects. Although the chlorophyll estimation model did not enable precise quantification under continuous monitoring, the sensor successfully detected substantial increases in chlorophyll associated with algae injections, demonstrating its potential for identifying algal bloom-like events.

Some limitations were identified, including the reliance on total chlorophyll measurements, whereas national regulations and trophic indices focus on chlorophyll-a and the absence of in situ validation. Despite these limitations, the prototype successfully demonstrated the feasibility of combining turbidity monitoring and algae detection in a single, low-cost optical device.

Answering the research question, the findings indicate that the proposed probe can distinguish between different sources of turbidity, but it loses accuracy and classification ability to a certain degree, under continuous monitoring scenarios, corroborating the second hypothesis. During the calibration stage for the $80-200$ NTU interval and throughout the continuous tests, MAE values above 5 NTU were observed, contradicting the initial hypothesis.Nevertheless, the low-cost sensor is a viable basis for affordable, continuous environmental monitoring, particularly in applications requiring early detection of turbidity fluctuations or algal bloom onset.

Future work could focus on the probe's design optimization, with the addition of an internal wiper, and the eventual removal of the maze-like pattern. Other possible paths, consist on refining the chlorophyll estimation model, adapting it for chlorophyll-a, and conducting long-term field deployments to assess performance under real environmental conditions. Further ahead, stages such as integration with different sensors (e.g. spectrometer and thermometer), as well as the configuration and implementation of a communication protocol (e.g. LoRaWAN and MQTT) for sending the obtained data, can be structured in order to further expand the scope of application for the sensor.

# References


ADJOVU, G. E.; STEPHEN, H.; JAMES, D.; AHMAD, S. *Overview of the Application of Remote Sensing in Effective Monitoring of Water Quality Parameters*. [S.l.]: MDPI, 2023.

AZIS, A.; YUSUF, H.; FAISAL, Z.; SURADI, M. Water turbidity impact on discharge decrease of groundwater recharge in recharge reservoir. In: *Procedia Engineering*. [S.l.]: Elsevier Ltd, 2015. v. 125, p. 199–206. ISSN 18777058.

BLOESCH, J. A review of methods used to measure sediment resuspension. *Hydrobiologia*, v. 284, n. 1, p. 13–18, 5 1994. ISSN 0018-8158.

BOWMAN, W.; HACKER, S.; CAIN, M. L. *Ecology*. 4. ed. [S.l.]: Sinauer Associates, 2017. 598 p. ISBN 9781605356181.

BUENO, R. de C.; DINIZ, A. L.; SANTOS, D.; BLENINGER, T. *AN IOT BASED LOW-COST TURBIDITY PROBE AND THE INFLUENCE OF COLOR LIGHT EMITTER AND MICROCONTROLLER RESOLUTION*. [S.l.], 2023. https://www.researchgate.net/publication/374002086.

CARPENTER, S. R.; CARACO, N. F.; CORRELL, D. L.; HOWARTH, R. W.; SHARPLEY, A. N.; SMITH, V. H. Nonpoint Pollution of Surface Waters with Phosphorus and Nitrogen. *Ecological Applications*, Wiley, v. 8, n. 3, p. 559, 8 1998. ISSN 10510761.

CHRISTENSEN, J.; LINDEN, K. G. How particles affect UV light in the UV Disinfection of Unfiltered Drinking Water. *Journal AWWA*, v. 95, n. 4, p. 179–189, 4 2003. ISSN 0003-150X.

DROUJKO, J.; MOLNAR, P. *Open-Source, Low-Cost, In-Situ Turbidity Sensor for River Network Monitoring*. 2021. https://www.researchsquare.com/article/rs-1181854/v1.

DUNAJSKI, M. V. L.; TULIO, A. E.; LUIZ, .; LUZ, H. N. F.; BUENO, . R. D. C.; BLENINGER, T. AVALIAÇÃO DO PROTOCOLO DE CALIBRAÇÃO DE TURBIDÍMETROS DE BAIXO-CUSTO PARA DETECÇÃO DE ALGAS EM CORPOS D'ÁGUA. In: . [S.l.: s.n.], 2023. ISSN 2318-0358.

FALCADE, D.; MANNICH, M.; COLOMBO, G. Tubo de turbidez para determinação de baixo custo da turbidez em corpos d-água superficiais. *Revista de Gestão de Água da América Latina*, Associacao Brasileira de Recursos Hidricos - ABRH, v. 14, n. 1, p. 5–5, 8 2017.

FISCHER, S.; FROMMEN, J. G. Eutrophication alters social preferences in three-spined sticklebacks (Gasterosteus aculeatus). *Behavioral Ecology and Sociobiology*, Springer Verlag, v. 67, n. 2, p. 293–299, 2 2013. ISSN 03405443.

GILLETT, D.; MARCHIORI, A. A low-cost continuous turbidity monitor. *Sensors (Switzerland)*, MDPI AG, v. 19, n. 14, 7 2019. ISSN 14248220.

GULLIAN, M.; ESPINOSA-FALLER, F. J.; NÚÑEZ, A.; LÓPEZ-BARAHONA, N. Effect of turbidity on the ultraviolet disinfection performance in recirculating aquaculture systems with low water exchange. *Aquaculture Research*, v. 43, n. 4, p. 595–606, 3 2012. ISSN 1355557X.

HECKY, R. E.; KILHAM, P.; SMITH, . S. V.; SCHINDLER, D. W.; HEALEY, F. P.; BRUNSKILL, G. J.; PATALAS, K.; FEE, E. J.; CAMPBELL, P. *Nutrient limitation of phytoplankton in freshwater and marine environments: A review of recent evidence on the effects of enrichment1*. [S.l.], 1988. v. 33, n. 4, 196–822 p.

Instituto Mineiro de Gestão das Águas (IGAM). *Índice de qualidade das águas*. https://igam.mg.gov.br/w/indice-de-qualidade-das-aguas-iqa.

KEELER, B. L.; POLASKY, S.; BRAUMAN, K. A.; JOHNSON, K. A.; FINLAY, J. C.; O'NEILLE, A.; KOVACS, K.; DALZELL, B. Linking water quality and well-being for improved assessment and valuation of ecosystem services. *Proceedings of the National Academy of Sciences of the United States of America*, v. 109, n. 45, p. 18619–18624, 11 2012. ISSN 00278424.

KELLEY, C. D.; KROLICK, A.; BRUNNER, L.; BURKLUND, A.; KAHN, D.; BALL, W. P.; WEBER-SHIRK, M. An affordable open-source turbidimeter. *Sensors (Switzerland)*, MDPI AG, v. 14, n. 4, p. 7142–7155, 4 2014. ISSN 14248220.

KLIMASZYK, P.; GOŁDYN, R. Water Quality of Freshwater Ecosystems in a Temperate Climate. *Water*, v. 12, n. 9, p. 2643, 9 2020. ISSN 2073-4441.

LECHEVALLIER, M. W.; EVANS, T. M.; SEIDLER, R. J. *Effect of Turbidity on Chlorination Efficiency and Bacterial Persistence in Drinking Water*. [S.l.], 1981. v. 42, n. 1, 159–167 p.

LIN, L.; YANG, H.; XU, X. *Effects of Water Pollution on Human Health and Disease Heterogeneity: A Review*. [S.l.]: Frontiers Media S.A., 2022.

MONTOYA-PACHONGO, C.; LOAIZA, D.; LOZADA, P. T.; CRUZ-VÉLEZ, C. H. *EFFECT OF INCREASE OF RAW WATER TURBIDITY ON EFFICIENCY OF CONVENTIONAL DRINKING WATER TREATMENT PROCESSES*. [S.l.]. https://www.researchgate.net/publication/317510784.

MURDOCH, P. S.; BARON, J. S.; MILLER, T. L. POTENTIAL EFFECTS OF CLIMATE CHANGE ON SURFACE-WATER QUALITY IN NORTH AMERICA <sup>1</sup>. *JAWRA Journal of the American Water Resources Association*, v. 36, n. 2, p. 347–366, 4 2000. ISSN 1093-474X.

O'MELIA, C. R. ES&T Features: Aquasols: the behavior of small particles in aquatic systems. *Environmental Science & Technology*, v. 14, n. 9, p. 1052–1060, 9 1980. ISSN 0013-936X.

PANAWALA, L. Home » Science » Biology » Cell Biology » Difference Between Chlorophyll A and B Difference Between Chlorophyll A and B Main Difference – Chlorophyll A vs Chlorophyll B. 6 2017.

PARRA, L.; ROCHER, J.; ESCRIVÁ, J.; LLORET, J. Design and development of low cost smart turbidity sensor for water quality monitoring in fish farms. *Aquacultural Engineering*, Elsevier B.V., v. 81, p. 10–18, 5 2018. ISSN 01448609.

ROCHER, J.; PARRA, L.; JIMENEZ, J. M.; LLORET, J.; BASTERRECHEA, D. A. Development of a low-cost optical sensor to detect eutrophication in irrigation reservoirs. *Sensors*, MDPI, v. 21, n. 22, 11 2021. ISSN 14248220.

SADAR, M. J. *Turbidity Science*. [S.l.]: Hach Company, 2003. v. 11. 1–26 p.

SANTANA, M. V. E.; ZHANG, Q.; MIHELCIC, J. R. Influence of Water Quality on the Embodied Energy of Drinking Water Treatment. *Environmental Science & Technology*, v. 48, n. 5, p. 3084–3091, 3 2014. ISSN 0013-936X.

SANTOS, E. Pedro dos. *DESENVOLVIMENTO DE UM SENSOR DE BAIXO CUSTO PARA ANÁLISE DA TURBIDEZ DA ÁGUA EM ALTA RESOLUÇÃO TEMPORAL*. (Doctoral dissertation) — Universidade Federal do Paraná, Curitiba, 2022.

United Nations. *Draft International Declaration of Human Rights*. 1948.

United Nations. *Transforming our world: the 2030 Agenda for Sustainable Development*. [S.l.], 2015.

VITOUSEK, P. M.; ABER, J. D.; HOWARTH, R. W.; LIKENS, G. E.; MATSON, P. A.; SCHINDLER, D. W.; SCHLESINGER, W. H.; TILMAN, D. G. *HUMAN ALTERATION OF THE GLOBAL NITROGEN CYCLE: SOURCES AND CONSEQUENCES*. [S.l.], 1997. v. 7, n. 3, 737–750 p.

VUILLEUMIER, C.; JEANNIN, P. Y.; HESSENAUER, M.; PERROCHET, P. Hydraulics and Turbidity Generation in the Milandre Cave (Switzerland). *Water Resources Research*, John Wiley and Sons Inc, v. 57, n. 8, 8 2021. ISSN 19447973.

World Health Organization. *Guidelines for drinking-water quality, , 4th edition, incorporating the 1st addendum*. [S.l.: s.n.], 2017. 541 p. ISBN 9789241549950.

World Health Organization. *Water quality and health-review of turbidity: information for regulators and water suppliers*. [S.l.]: World Health Organization, 2017.